

SUPPORTING INFORMATION

Heterobimetallic Ruthenium-Zinc Complexes with Bulky N-Heterocyclic Carbenes:
Syntheses, Structures and Reactivity

Maialen Espinal-Viguri, Victor Varela-Izquierdo, Fedor M. Miloserdov, Ian M. Riddlestone,
Mary F. Mahon and Michael K. Whittlesey

Department of Chemistry, University of Bath, Claverton Down, Bath BA2 7AY, UK

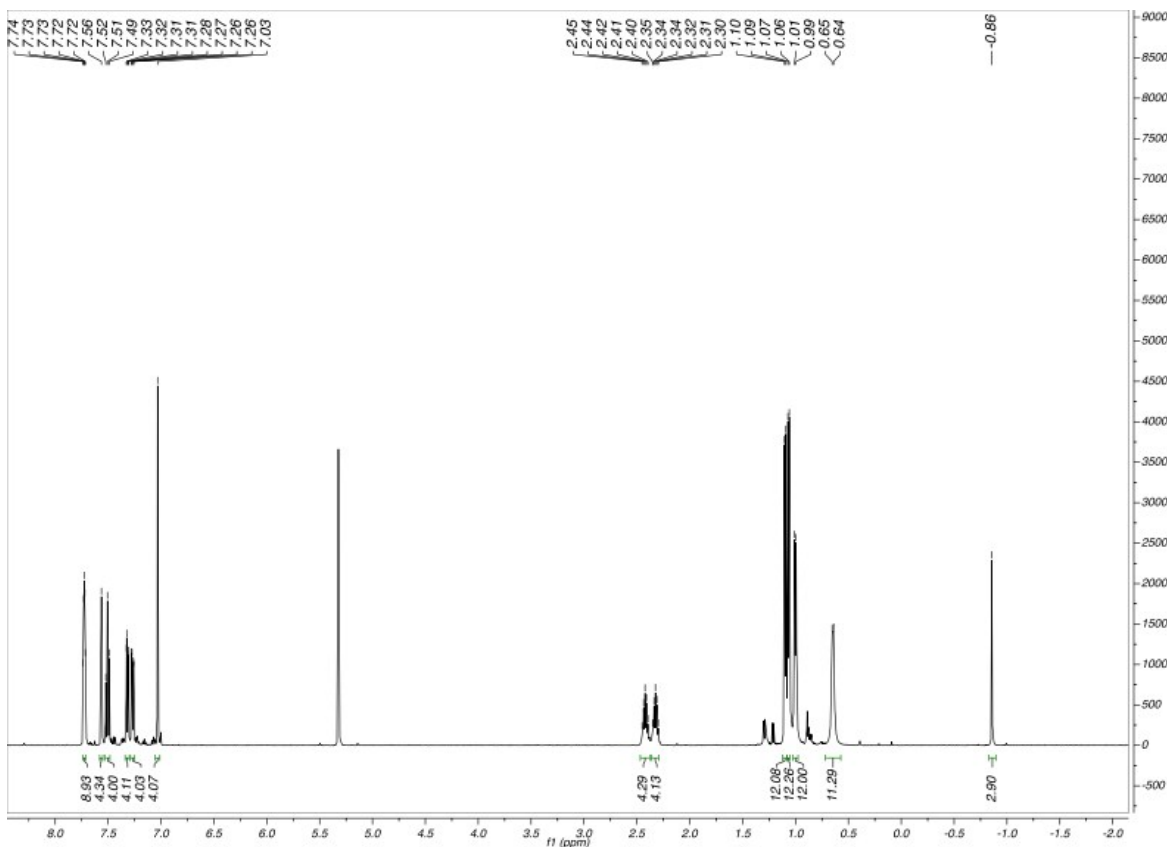


Figure S1. ^1H NMR spectrum (500 MHz, CD_2Cl_2 , 298 K) of $[\text{Ru}(\text{IPr})_2(\text{CO})\text{ZnMe}][\text{BArF}_4]$ (7).

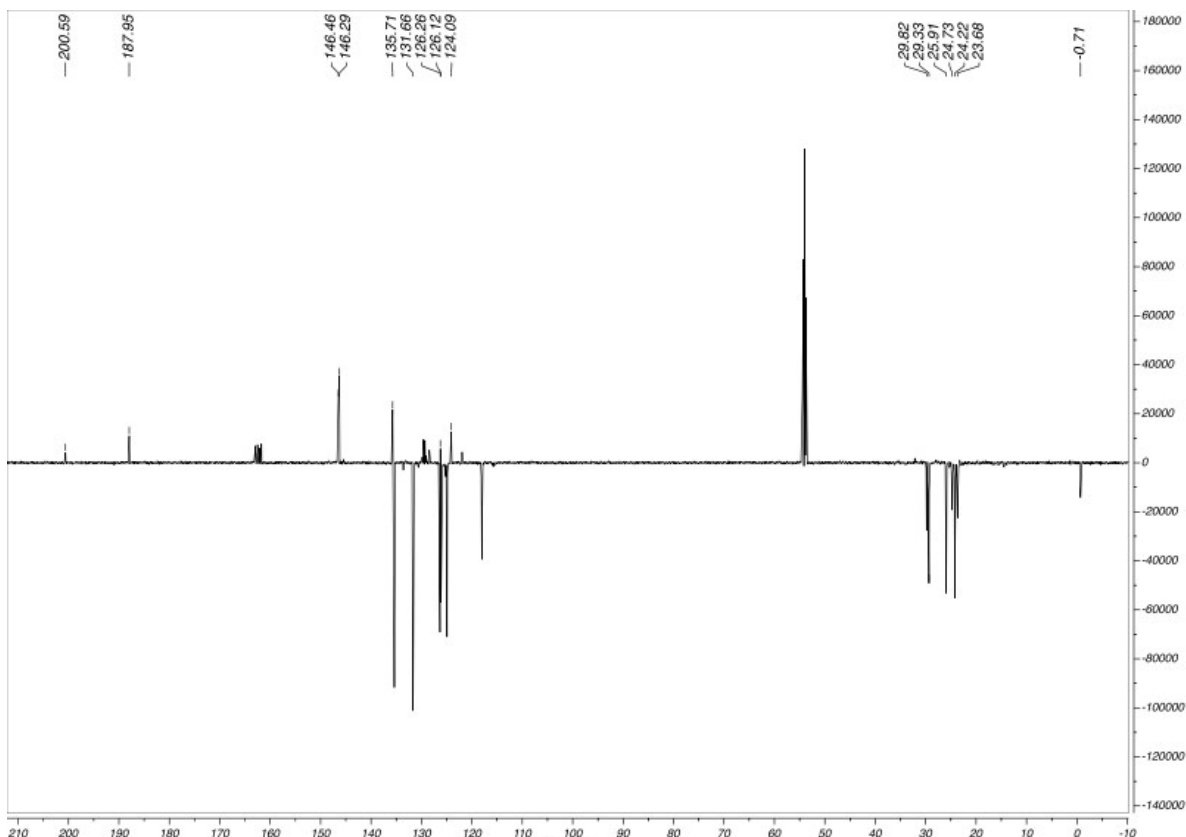


Figure S2. $^{13}\text{C}\{^1\text{H}\}$ PENDANT NMR spectrum (101 MHz, CD_2Cl_2 , 298 K) of $[\text{Ru}(\text{IPr})_2(\text{CO})\text{ZnMe}][\text{BArF}_4]$ (7).

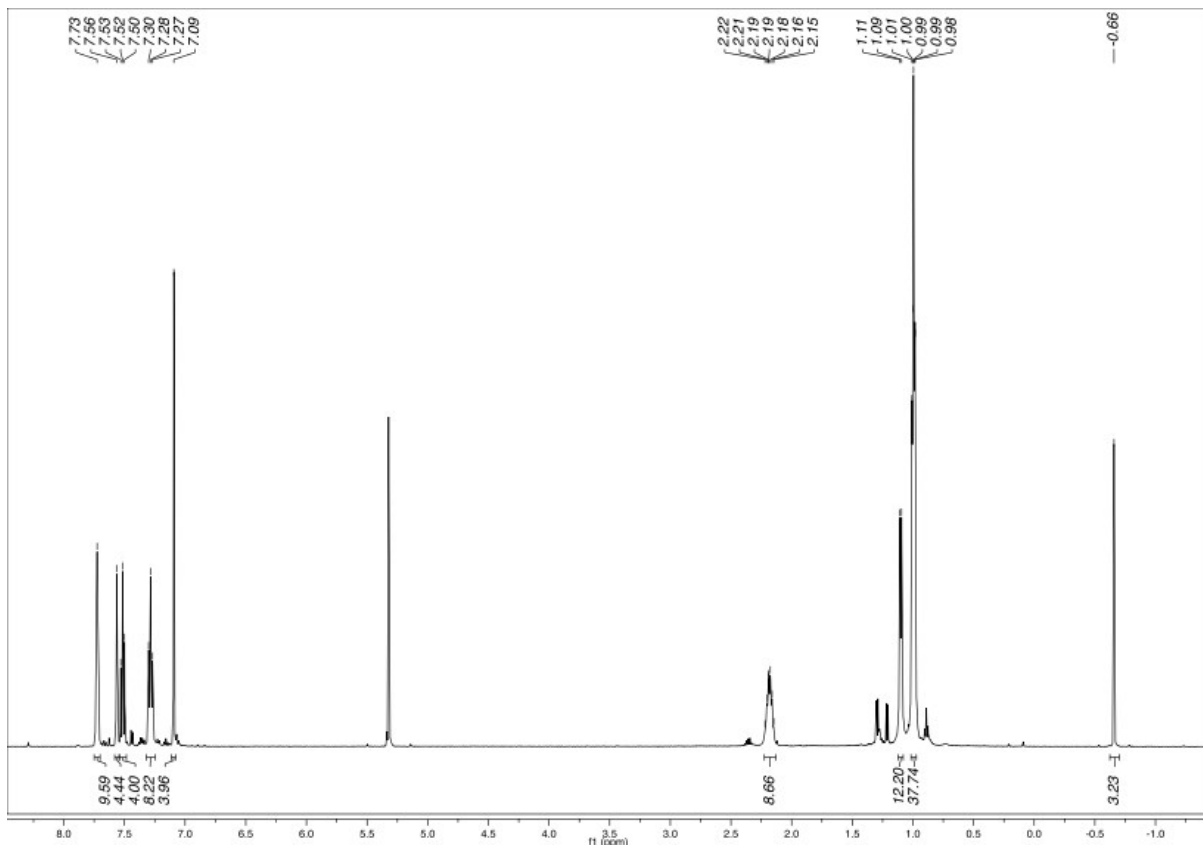


Figure S3. High frequency region of the ^1H NMR spectrum (500 MHz, CD_2Cl_2 , 298 K) of $[\text{Ru}(\text{IPr})_2(\text{CO})(\eta^2\text{-H}_2)(\text{H})_2\text{ZnMe}][\text{BAr}_4^{\text{F}}]$ (**8**).

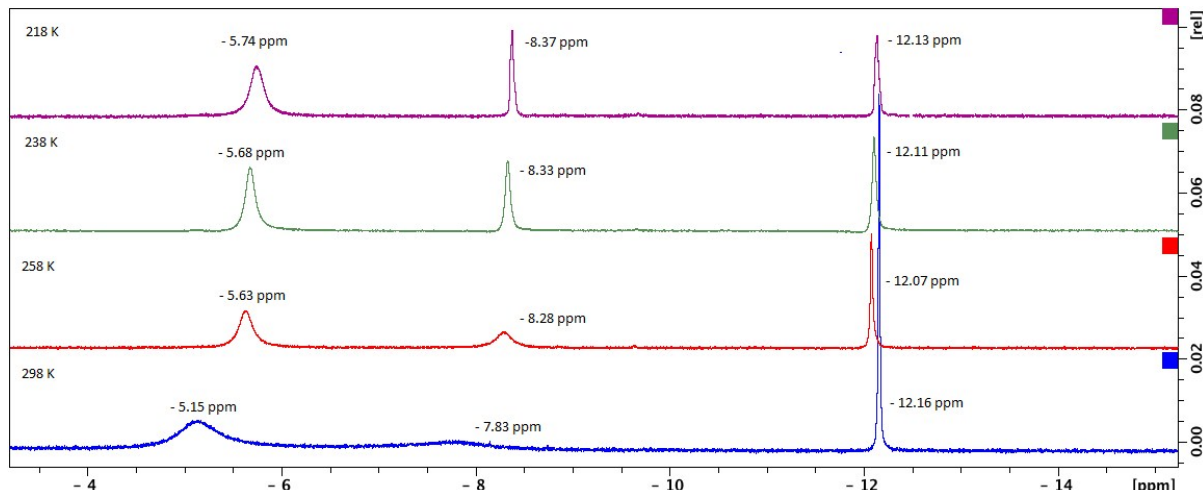


Figure S4. Variable temperature proton NMR spectra of the low frequency region of the ^1H NMR spectrum (500 MHz, CD_2Cl_2) of $[\text{Ru}(\text{IPr})_2(\text{CO})(\eta^2\text{-H}_2)(\text{H})_2\text{ZnMe}][\text{BAr}_4^{\text{F}}]$ (**8**).

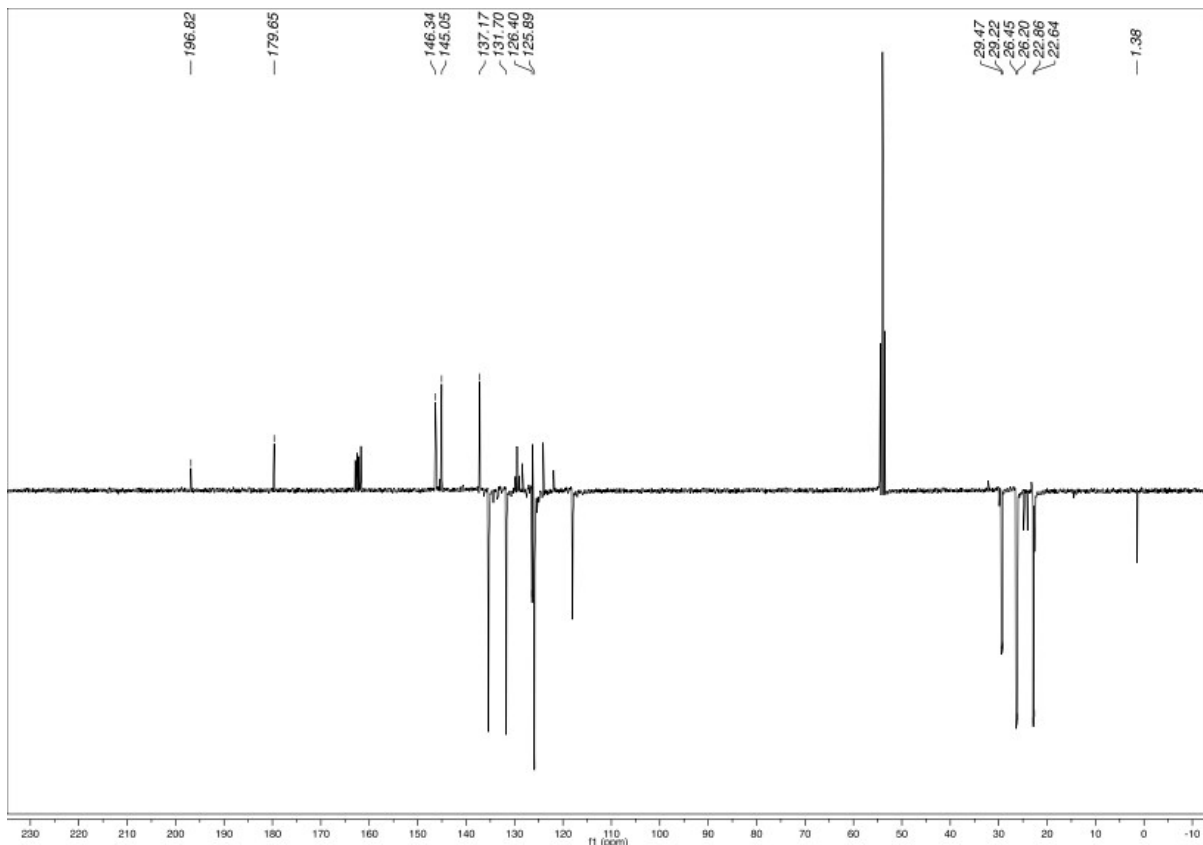


Figure S5. $^{13}\text{C}\{^1\text{H}\}$ PENDANT NMR spectrum (101 MHz, CD_2Cl_2 , 298 K) of $[\text{Ru}(\text{IPr})_2(\text{CO})(\eta^2\text{-H}_2)(\text{H})_2\text{ZnMe}][\text{BArF}_4]$ (**8**).

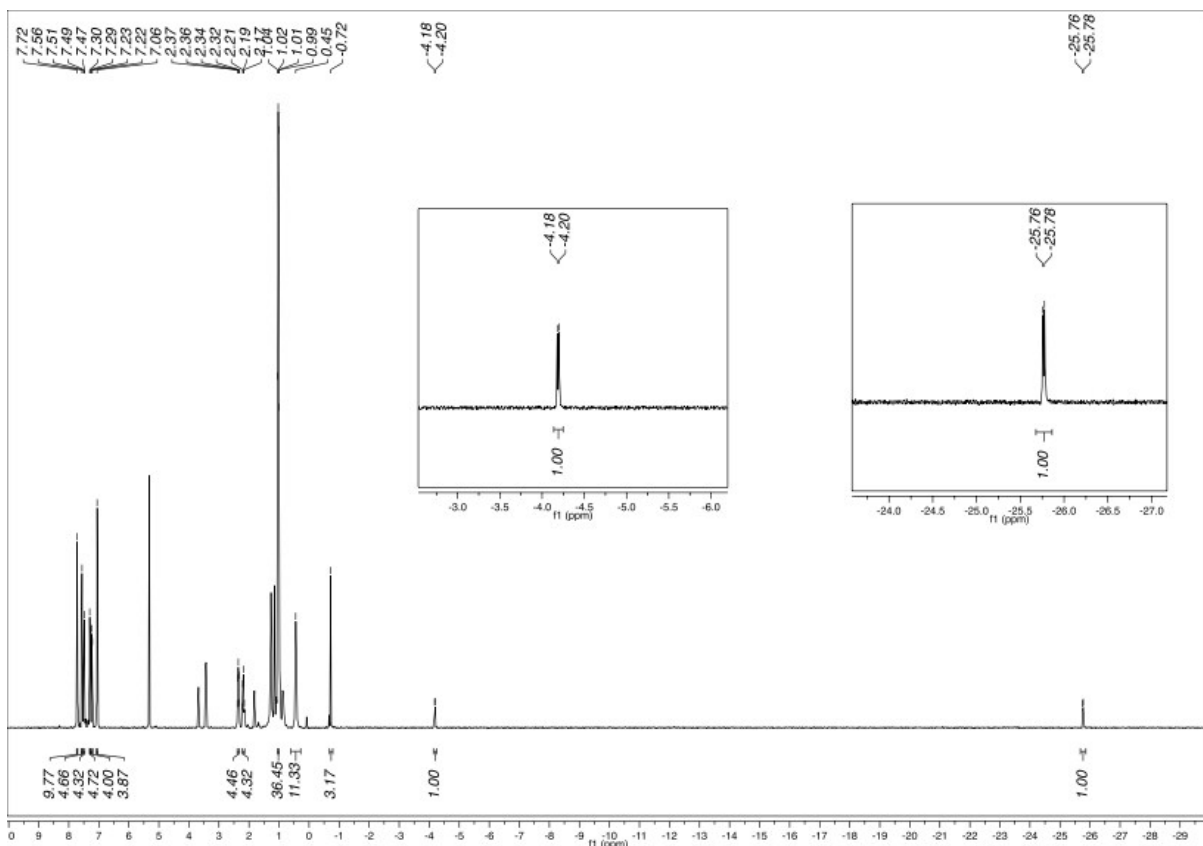


Figure S6. ^1H NMR spectrum (500 MHz, CD_2Cl_2 , 298 K) of $[\text{Ru}(\text{IPr})_2(\text{CO})(\text{H})_2\text{ZnMe}][\text{BArF}_4]$ (**9**).

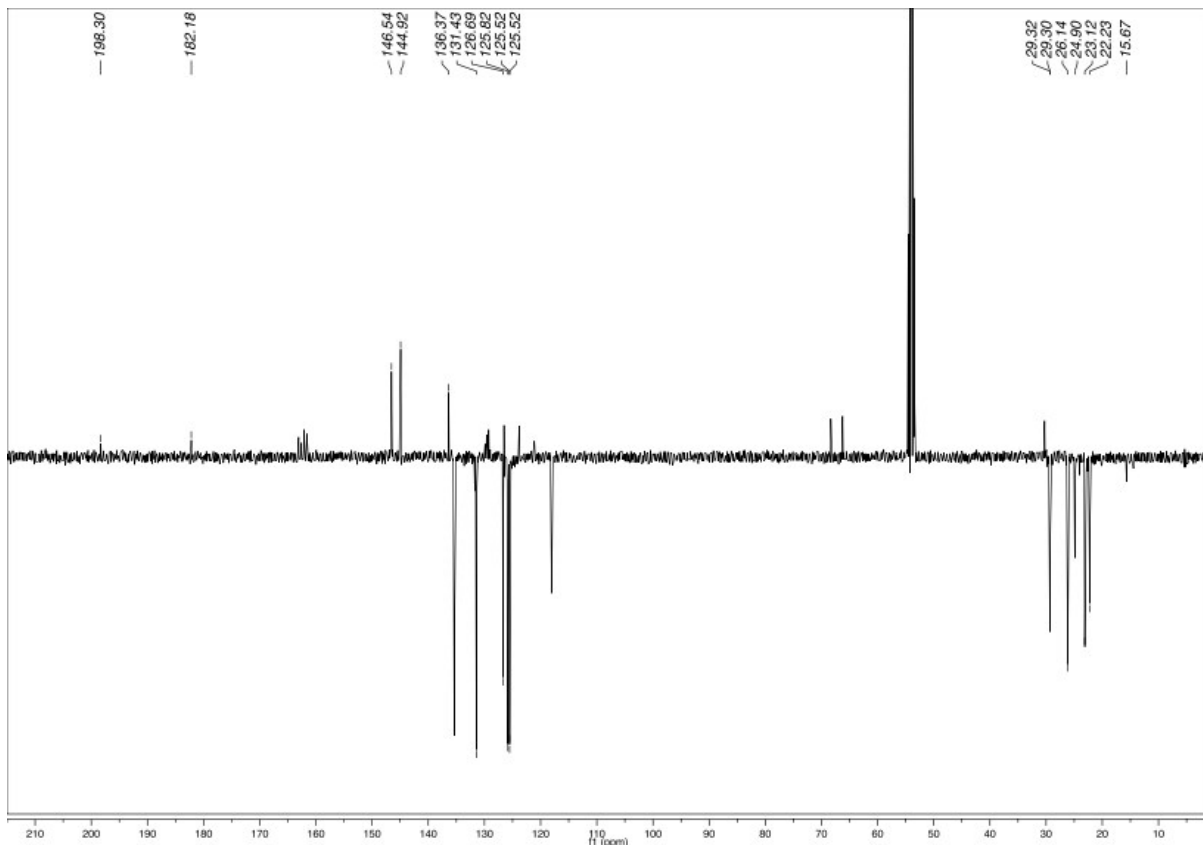


Figure S7. $^{13}\text{C}\{^1\text{H}\}$ PENDANT NMR spectrum (101 MHz, CD_2Cl_2 , 298 K) of $[\text{Ru}(\text{IPr})_2(\text{CO})(\text{H})_2\text{ZnMe}][\text{BArF}_4]$ (**9**).

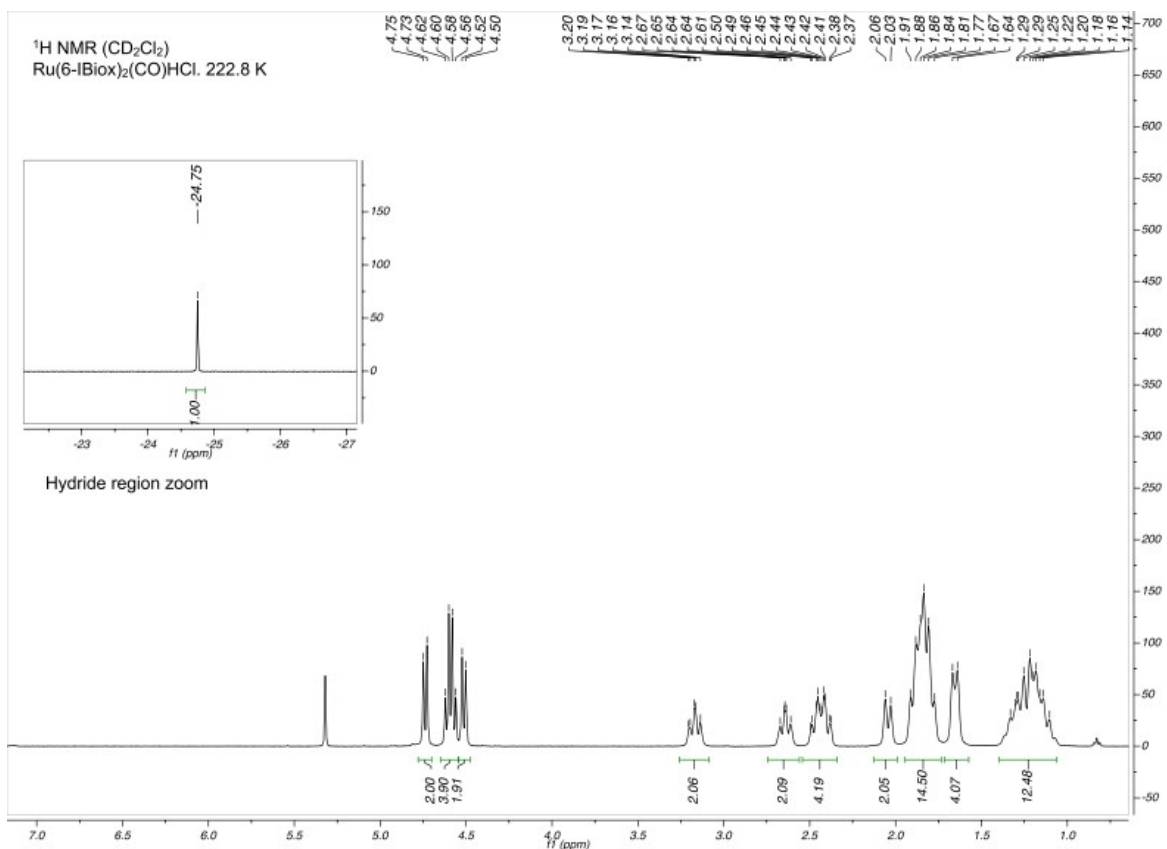


Figure S8. ^1H NMR spectrum (500 MHz, CD_2Cl_2 , 223 K) of $[\text{Ru}(\text{IBiox}_6)_2(\text{CO})\text{HCl}]$ (**10**).

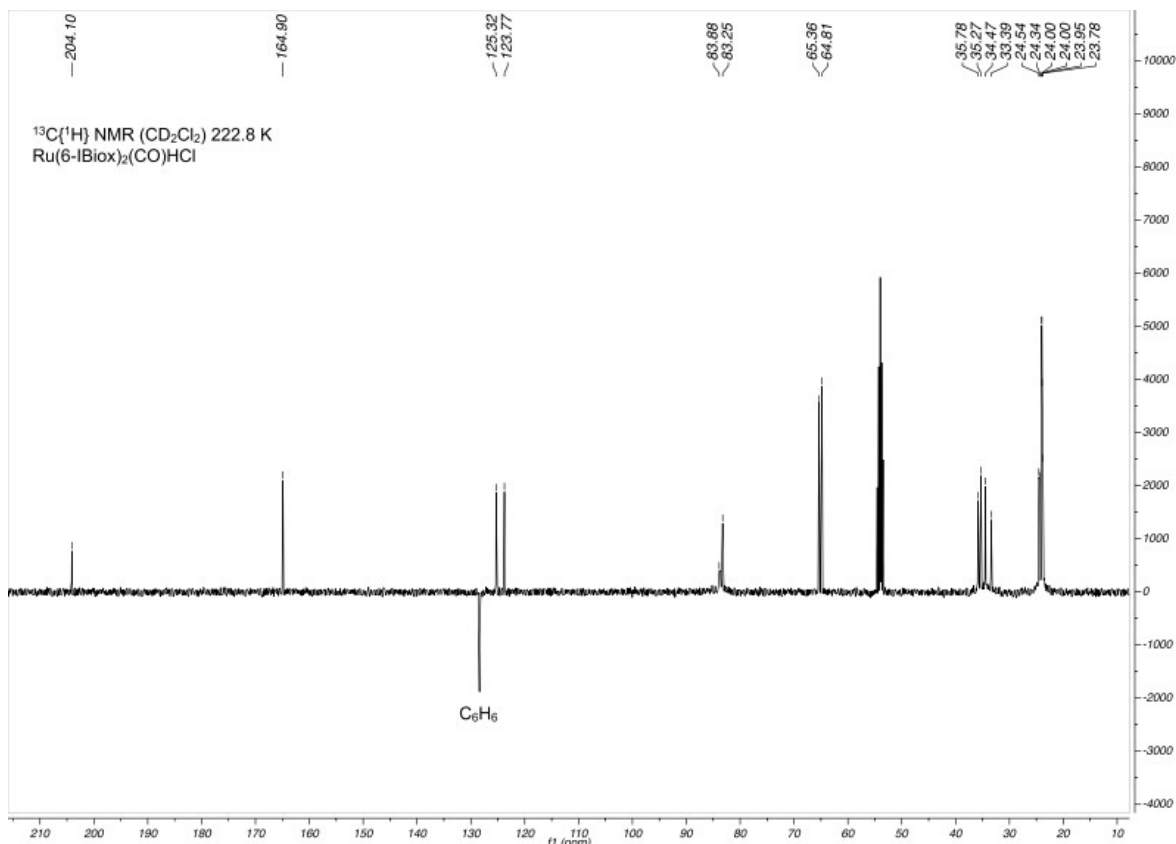


Figure S9. $^{13}\text{C}\{\text{H}\}$ PENDANT NMR spectrum (126 MHz, CD_2Cl_2 , 223 K) of $[\text{Ru}(\text{IBiox6})_2(\text{CO})(\text{HCl})]$ (**10**).

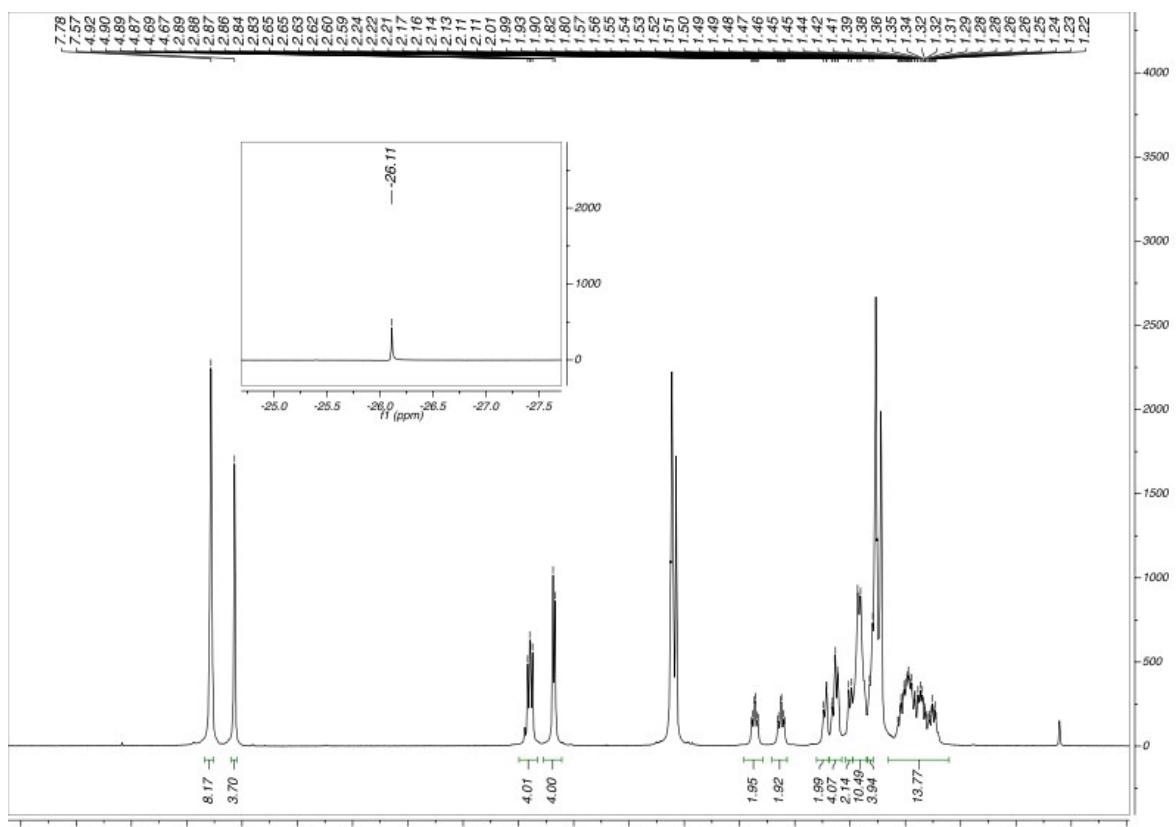


Figure S10. ^1H NMR spectrum (500 MHz, $\text{THF}-d_8$, 298 K) of $[\text{Ru}(\text{IBiox6})_2(\text{CO})(\text{THF})\text{H}][\text{BAr}^{\text{F}}_4]$ (**11**).

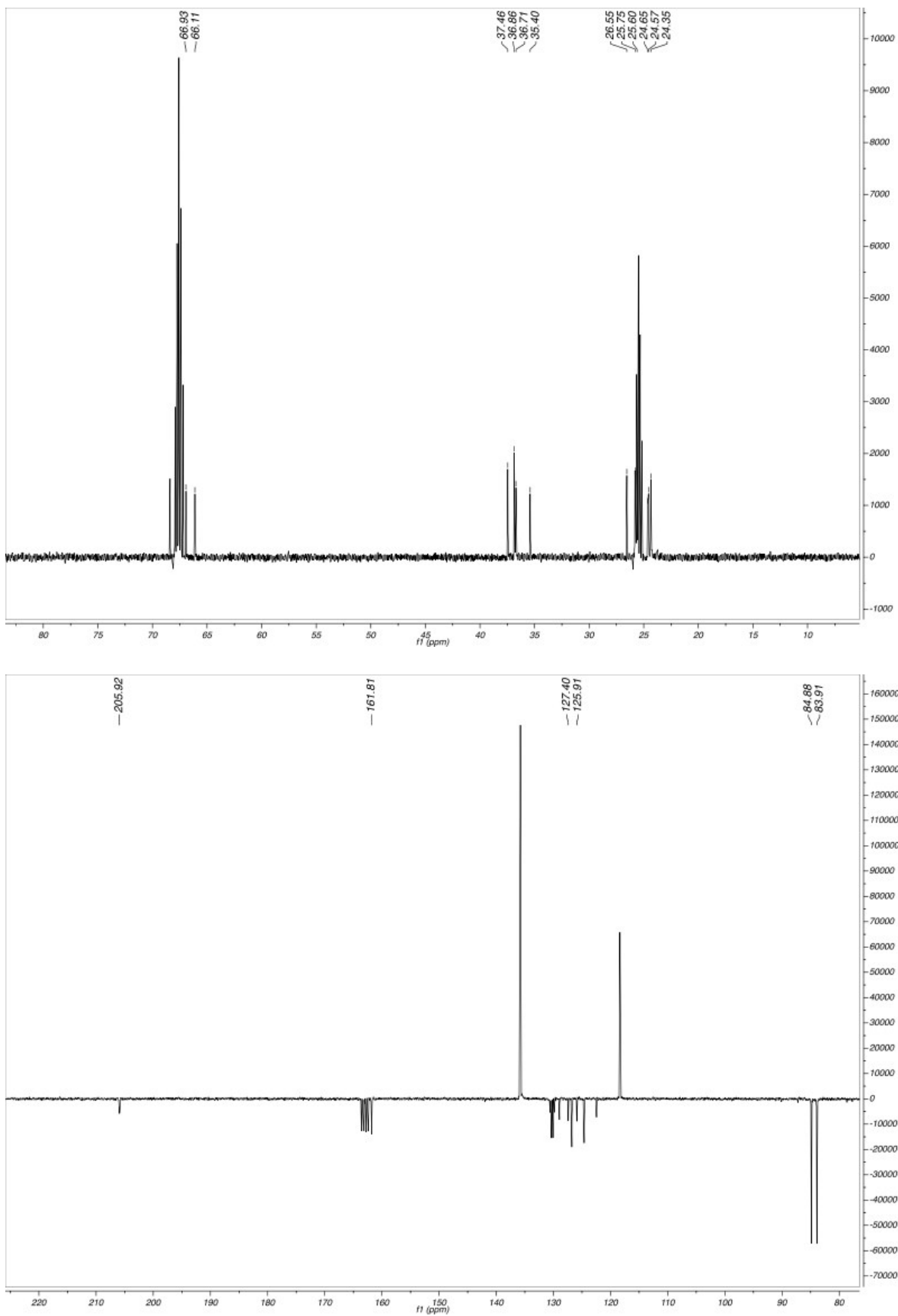


Figure S11. High (top) and lower (bottom) frequency regions of the $^{13}\text{C}\{{}^1\text{H}\}$ PENDANT NMR spectrum (126 MHz, THF- d_8 , 298 K) of $[\text{Ru}(\text{IBiox}_6)_2(\text{CO})(\text{THF})\text{H}][\text{BAr}^{\text{F}}_4]$ (**11**).

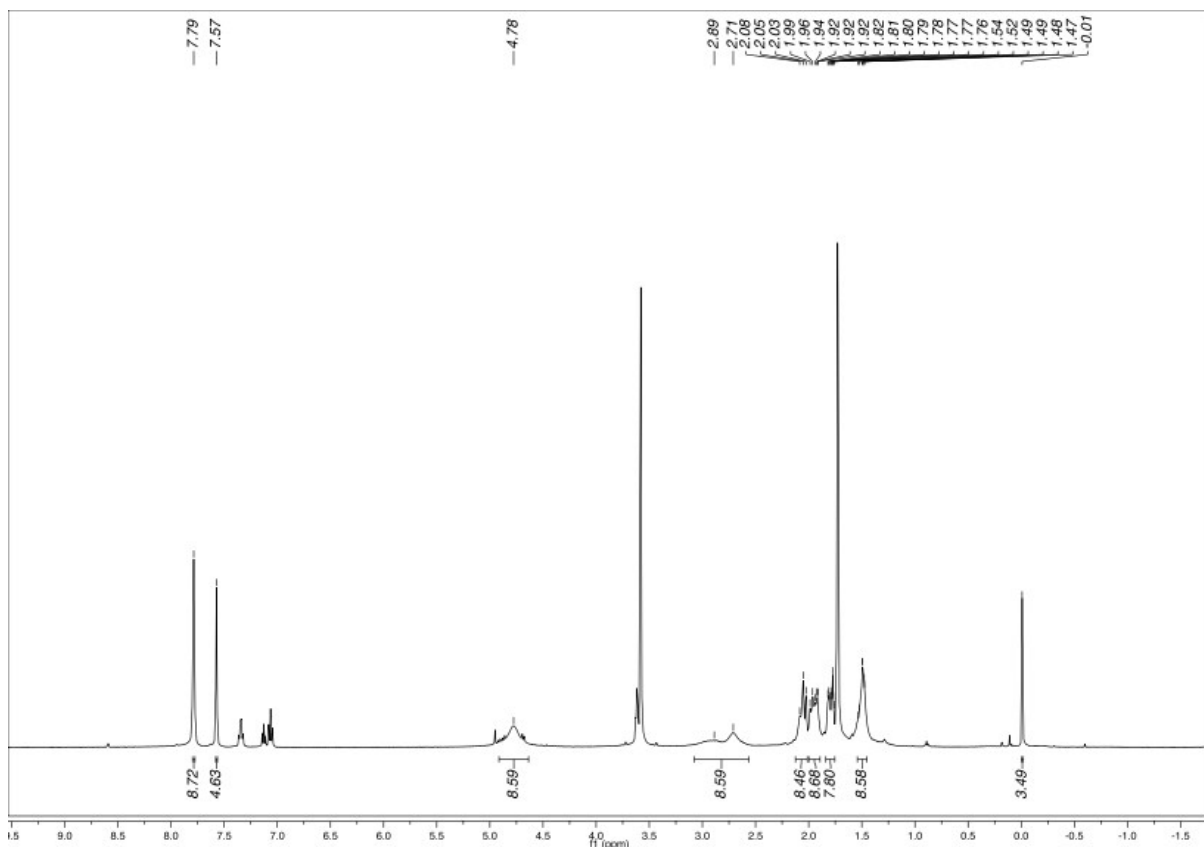


Figure S12. ^1H NMR spectrum (500 MHz, THF- d_8 , 298 K) of $[\text{Ru}(\text{IBiox}_6)_2(\text{CO})(\text{THF})\text{ZnMe}][\text{BAr}_4^{\text{F}}]$ (**12**).

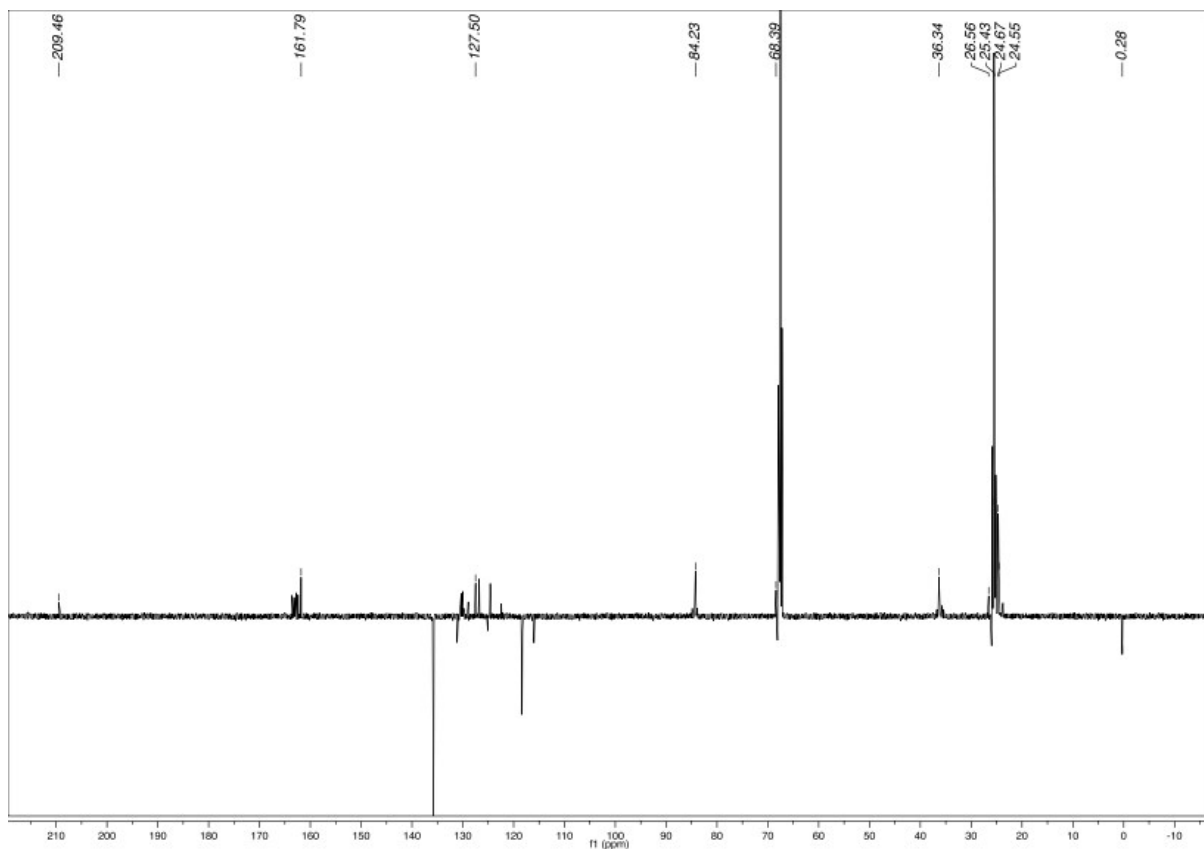


Figure S13. $^{13}\text{C}\{^1\text{H}\}$ PENDANT NMR spectrum (126 MHz, THF- d_8 , 298 K) of $[\text{Ru}(\text{IBiox}_6)_2(\text{CO})(\text{THF})\text{ZnMe}][\text{BAr}_4^{\text{F}}]$ (**12**).

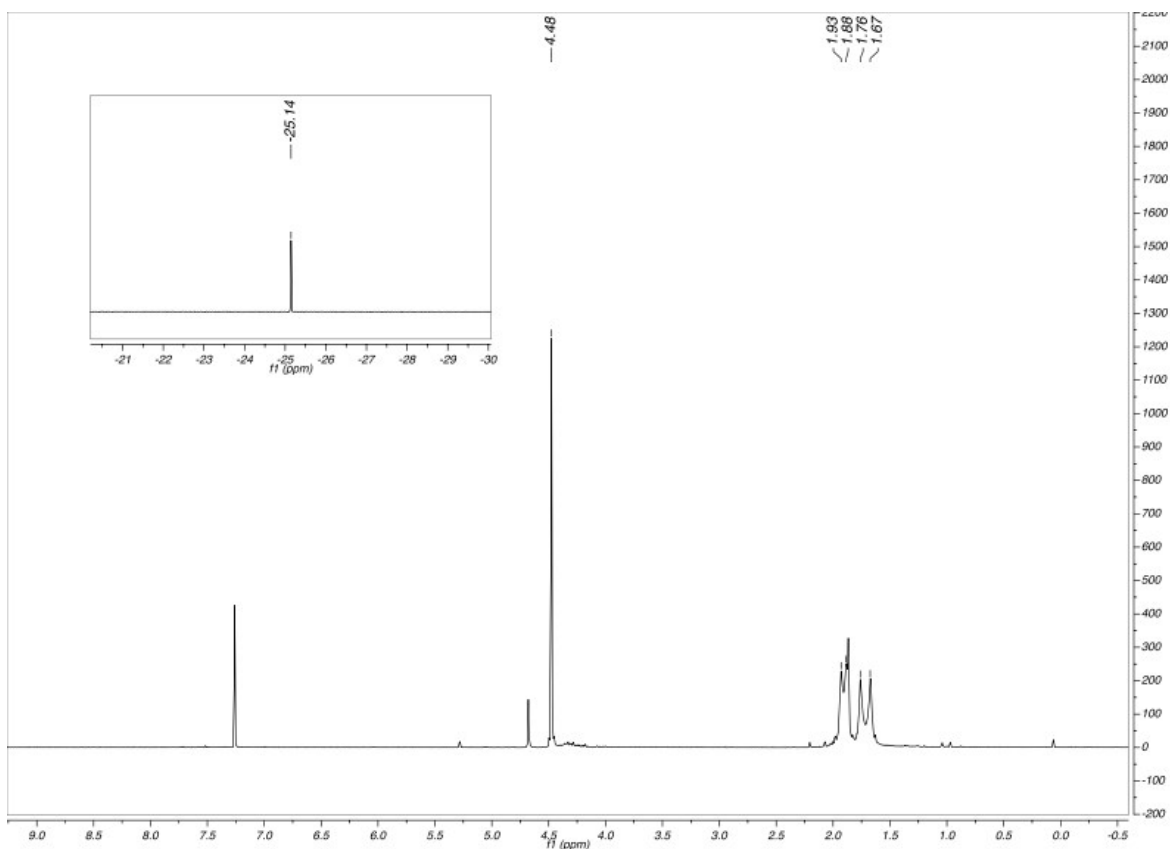


Figure S14. ¹H NMR spectrum (500 MHz, CDCl₃, 298 K) of [Ru(IBioxMe₄)₂(CO)HCl] (**13**).

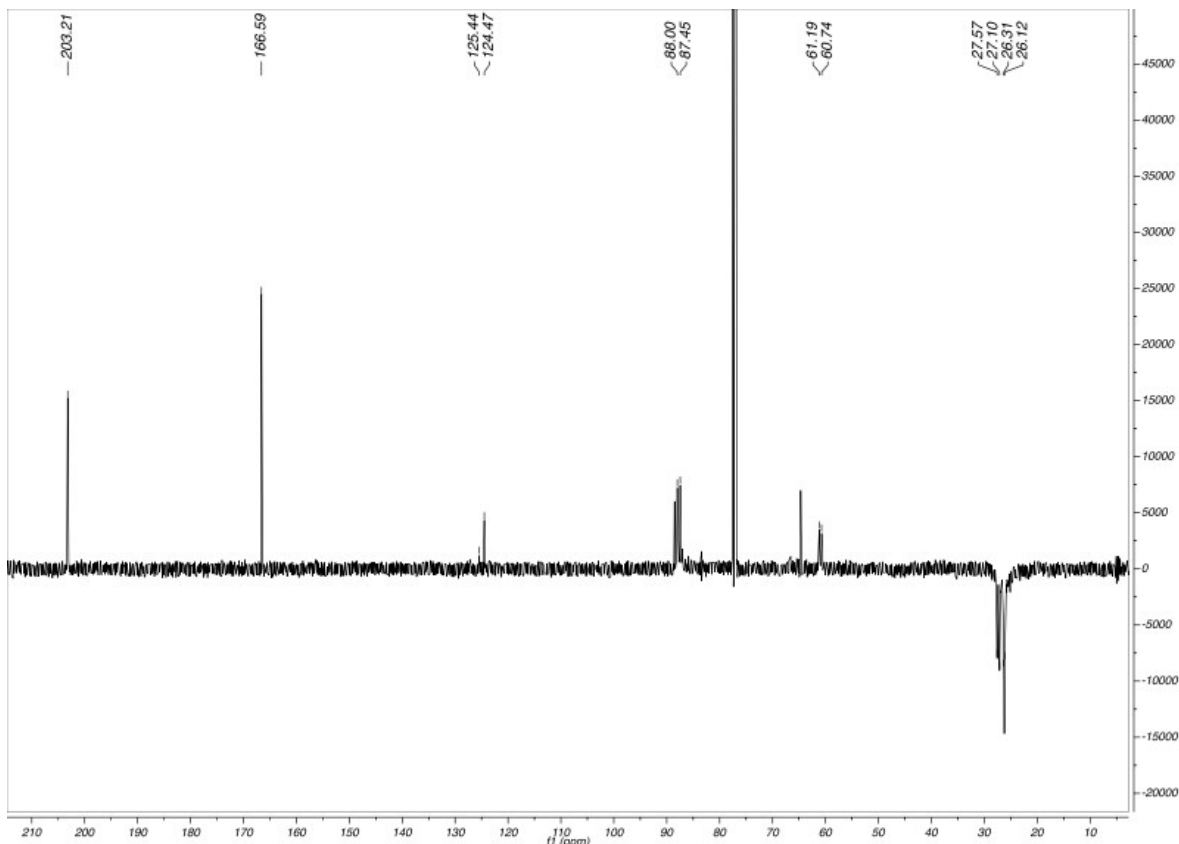


Figure S15. ¹³C{¹H} PENDANT NMR spectrum (126 MHz, CDCl₃, 298 K) of [Ru(IBioxMe₄)₂(CO)HCl] (**13**).

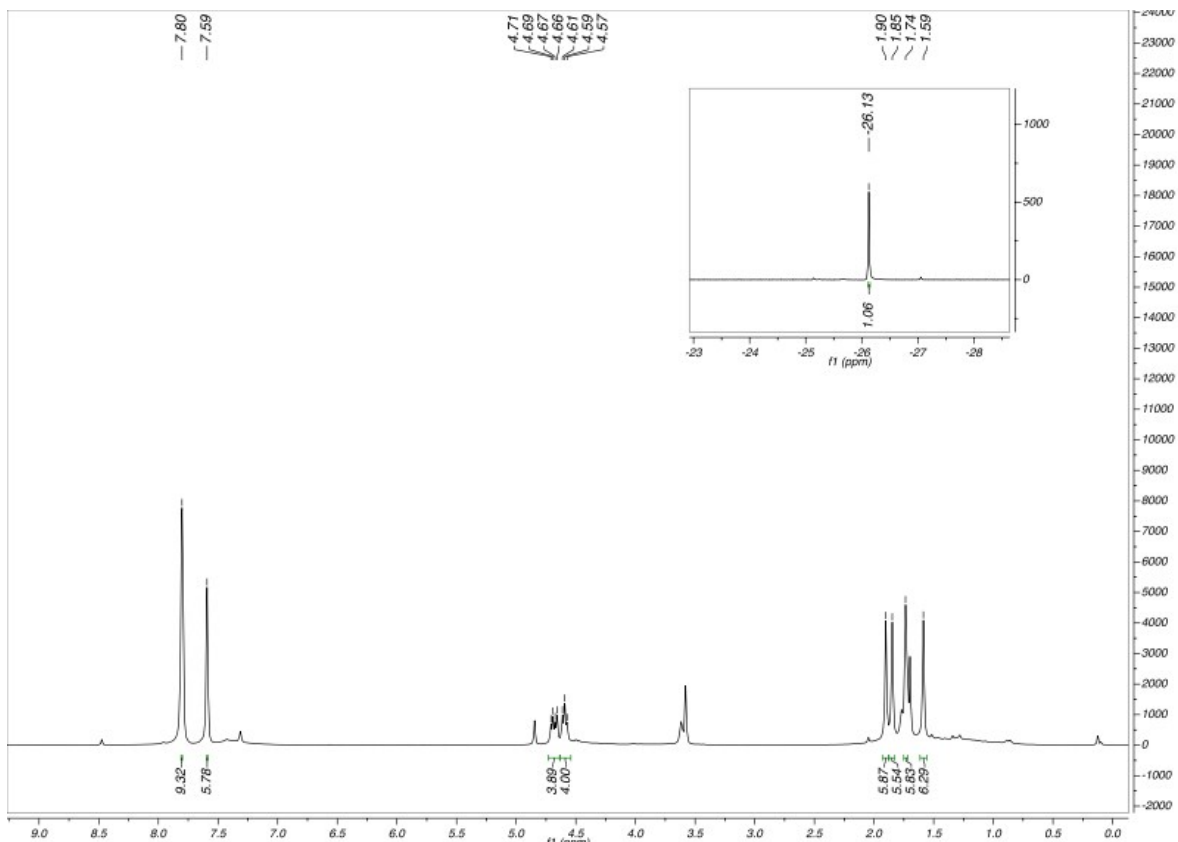


Figure S16. ^1H NMR spectrum (400 MHz, THF- d_8 , 298 K) of $[\text{Ru}(\text{IBioxMe}_4)_2(\text{CO})(\text{THF})\text{H}][\text{BAr}^{\text{F}}_4]$ (**14**).

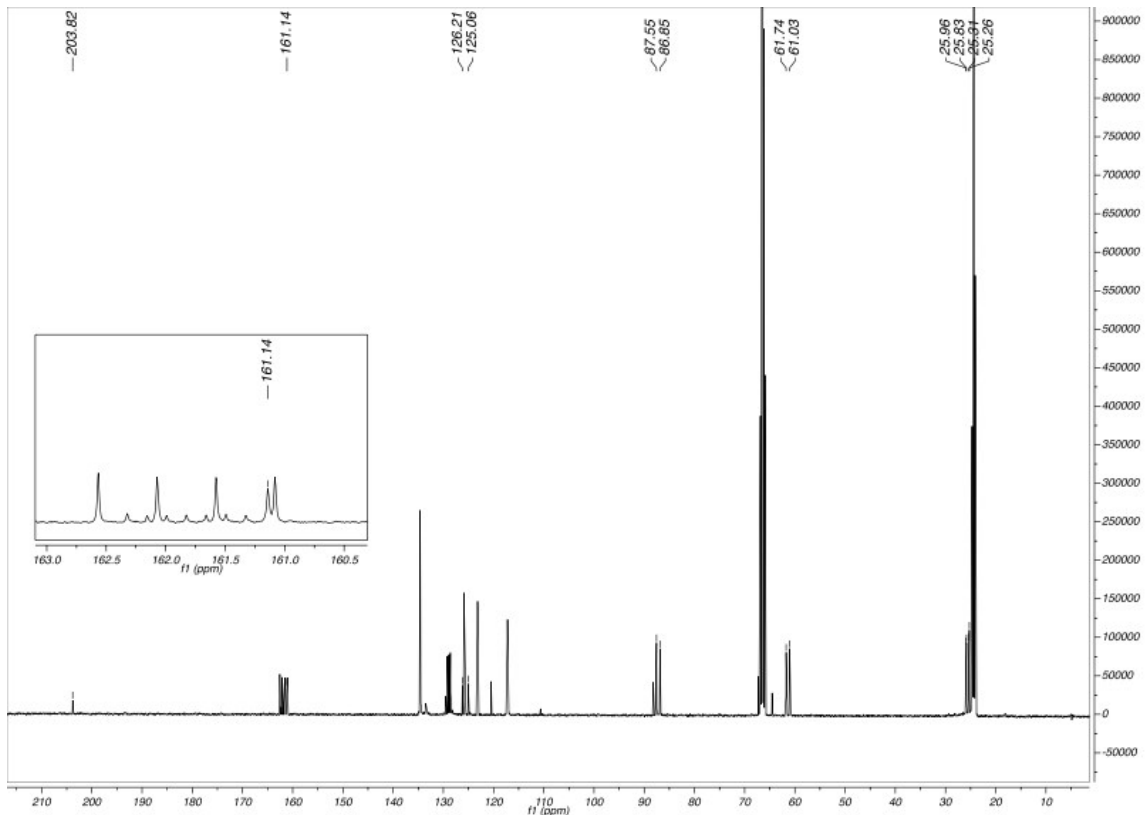


Figure S17. $^{13}\text{C}\{^1\text{H}\}$ NMR spectrum (101 MHz, THF- d_8 , 298 K) of $[\text{Ru}(\text{IBioxMe}_4)_2(\text{CO})(\text{THF})\text{H}][\text{BAr}^{\text{F}}_4]$ (**14**).

[Ru(IMes)(PPh₃)(CO)HCl]. The compound was synthesised by a minor modification of the literature procedure.¹ IMes (200 mg, 0.655 mmol) was added to the suspension of finely powdered [Ru(PPh₃)₃(CO)HCl]·CH₂Cl₂ (426 mg, 0.410 mmol) in toluene (5 mL). The solution was stirred overnight, after which time reaction was complete by ³¹P{¹H} NMR spectroscopy. The solvent was concentrated under vacuum to ca. 0.5 mL and treated with hexane (8 mL) at room temperature. A yellow-orange microcrystalline precipitate was filtered off, washed with hexane (3 x 5 mL) and dried under vacuum. Yield 256 mg (85%).

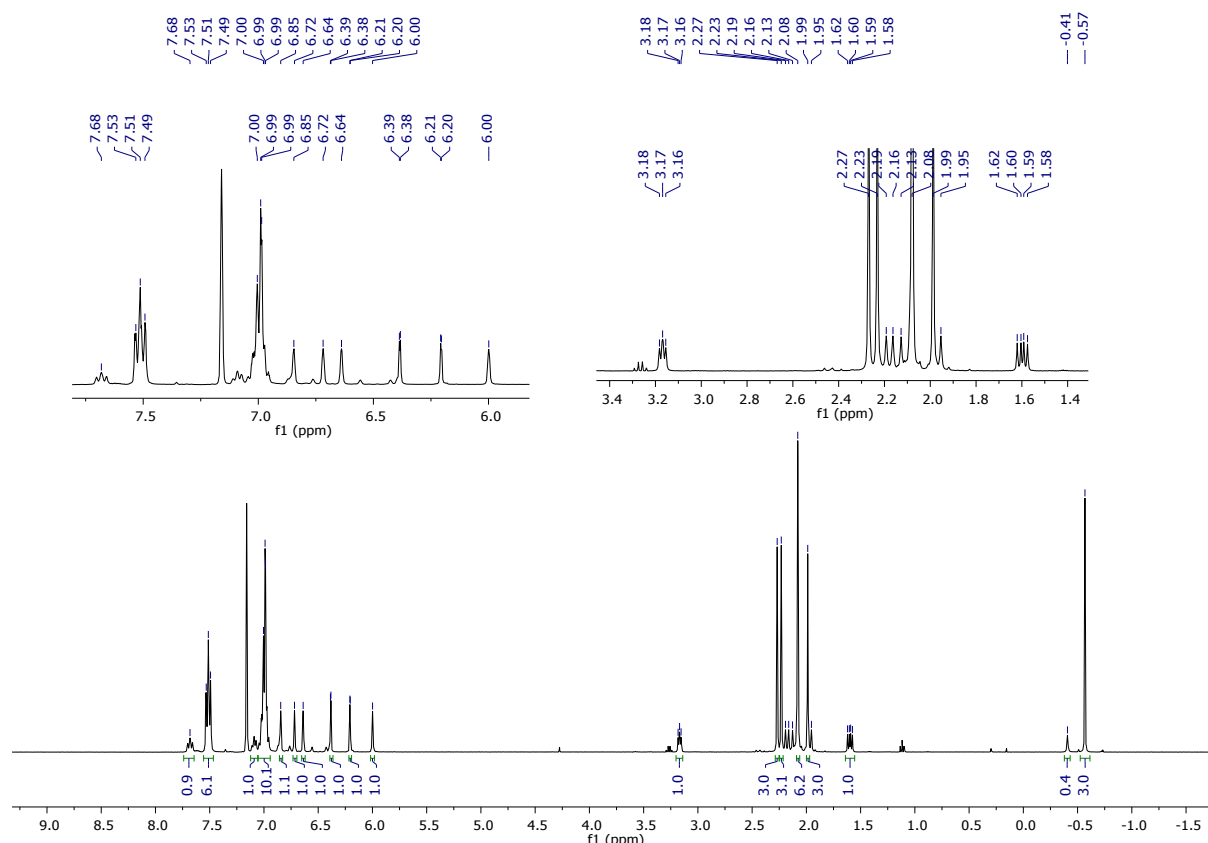


Figure S18. ^1H NMR spectrum (500 MHz, C_6D_6 , 298 K) of $[\text{Ru}(\text{IMes})'(\text{PPh}_3)(\text{CO})\text{ZnMe}]$ (15).

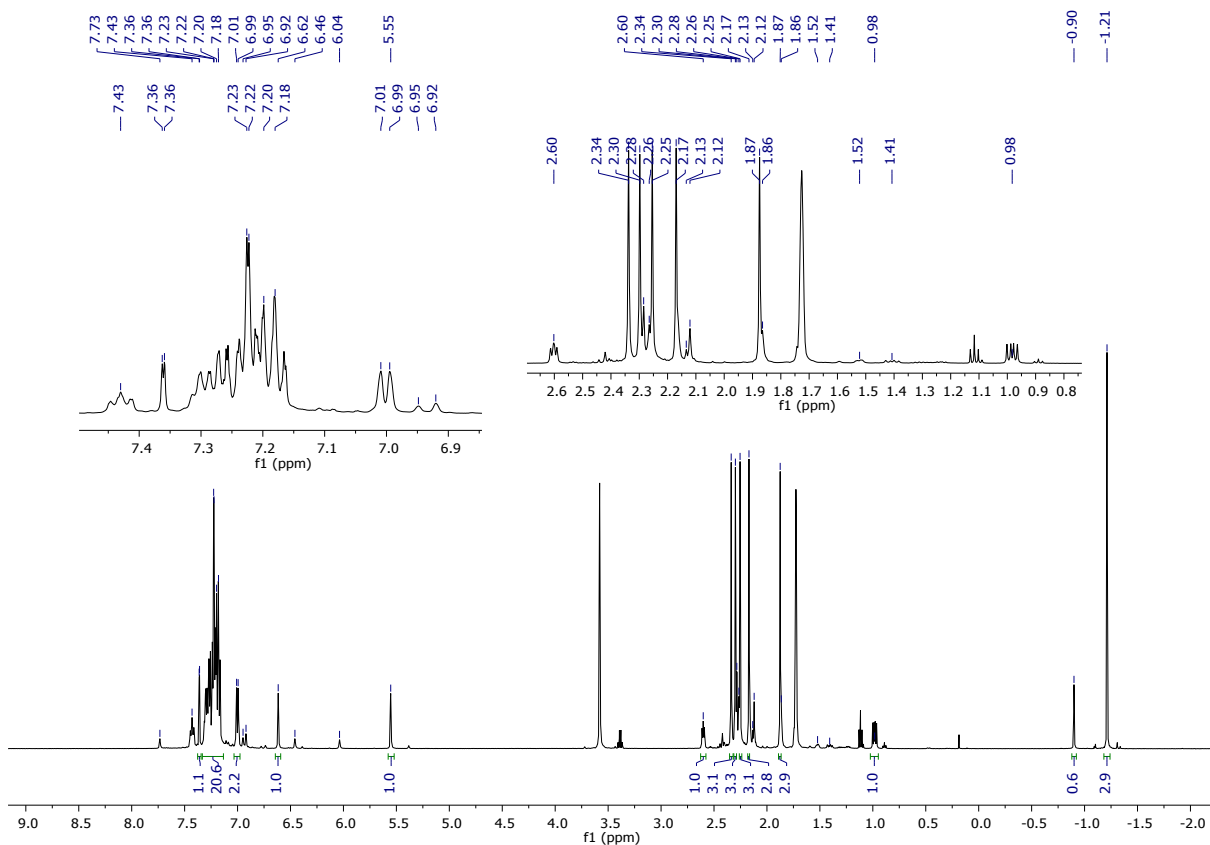


Figure S19. ¹H NMR spectrum (500 MHz, THF-*d*₈, 298 K) of [Ru(IMes')(PPh₃)(CO)ZnMe] (**15**).

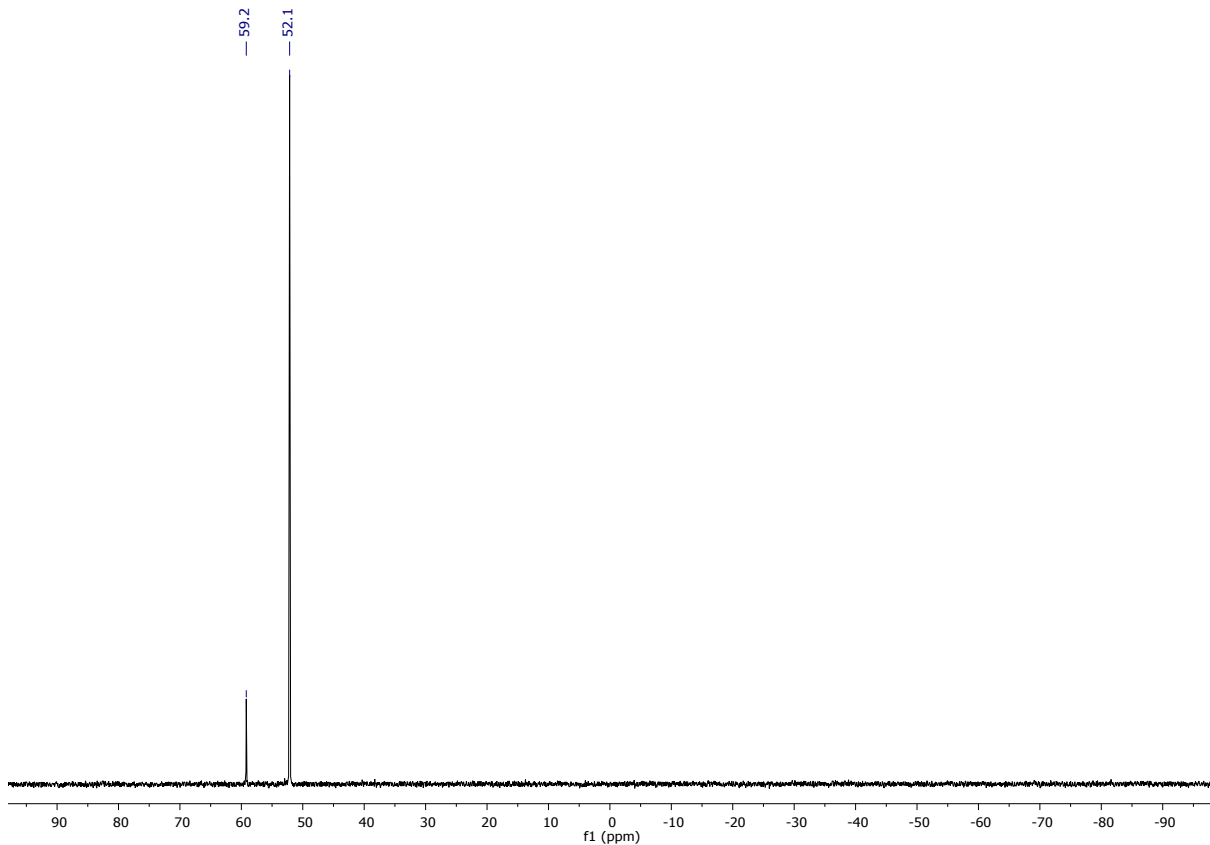


Figure S20. ³¹P{¹H} NMR spectrum (162 MHz, C₆D₆, 298 K) of [Ru(IMes')(PPh₃)(CO)ZnMe] (**15**).

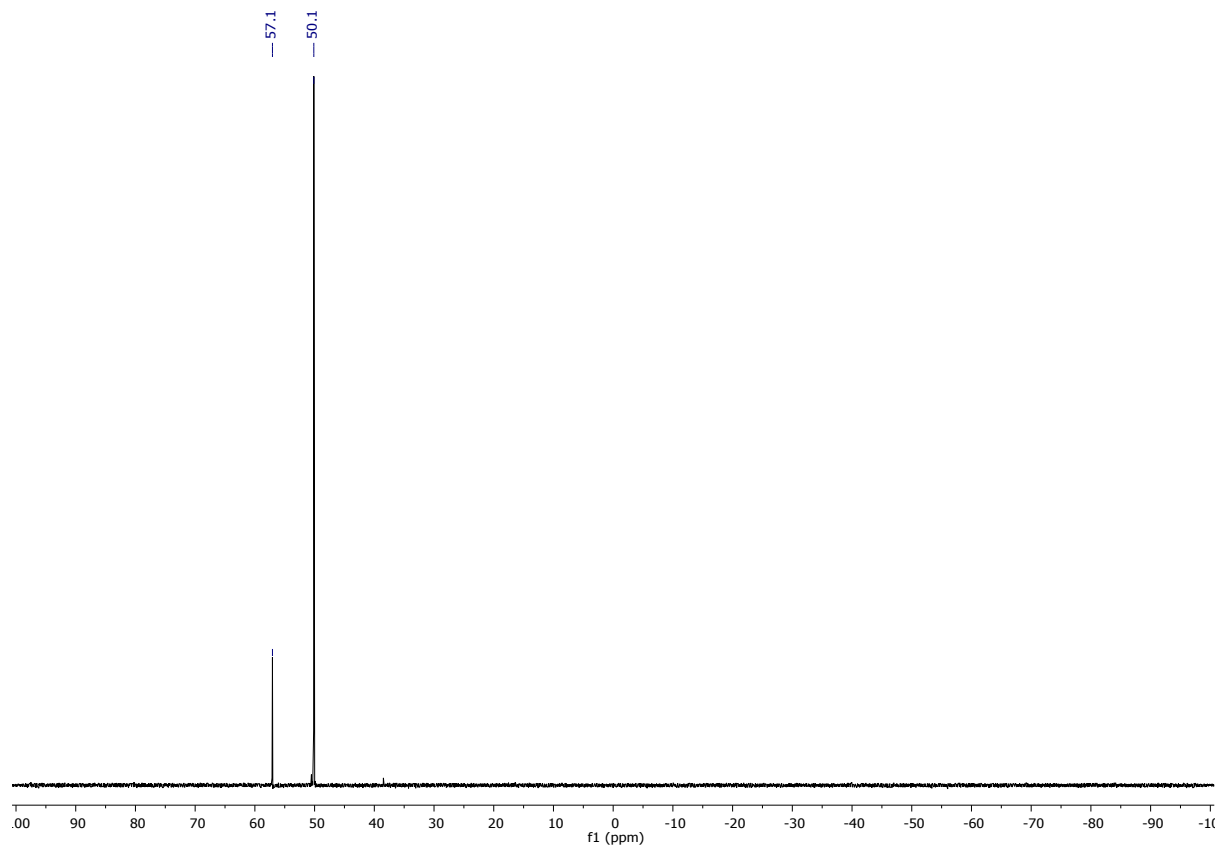


Figure S21. ${}^{31}\text{P}\{{}^1\text{H}\}$ NMR spectrum (162 MHz, THF- d_8 , 298 K) of $[\text{Ru}(\text{IMes})(\text{PPh}_3)(\text{CO})\text{ZnMe}]$ (15).

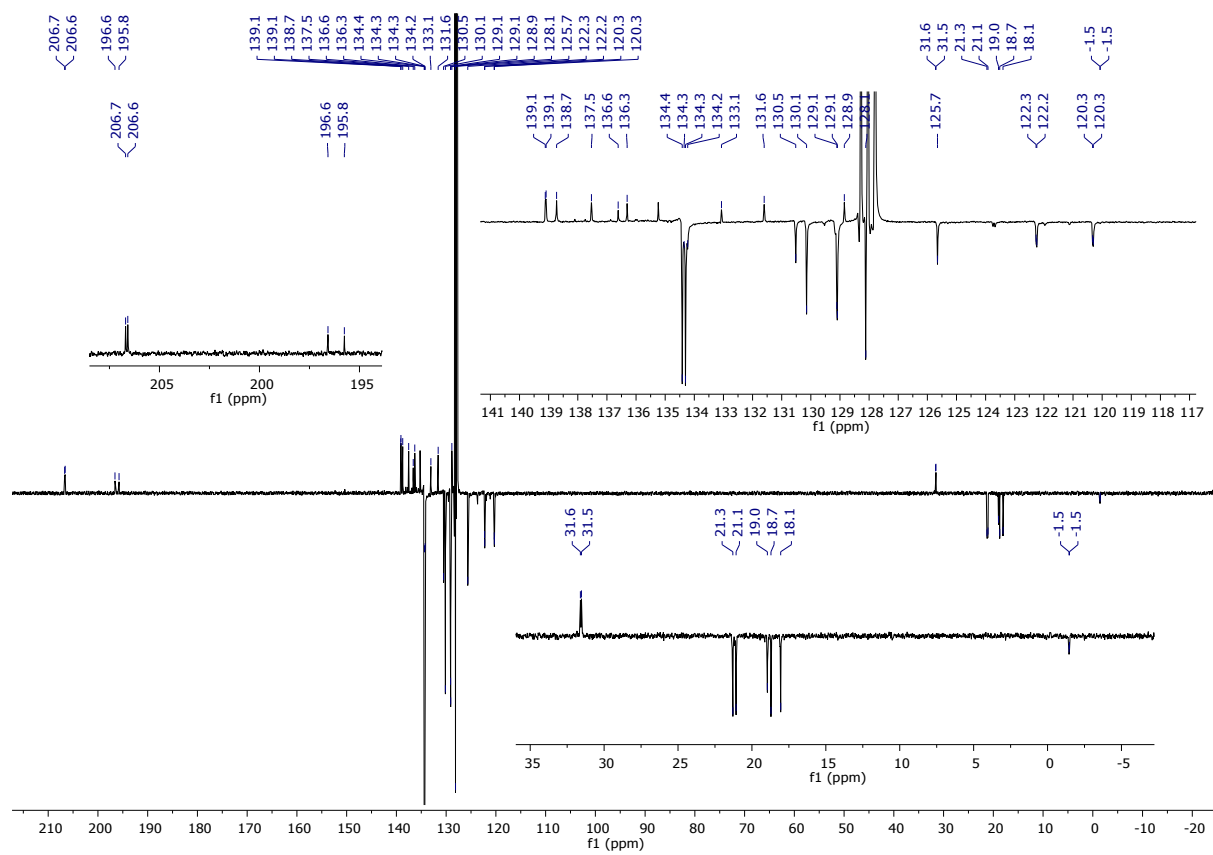


Figure S22. $^{13}\text{C}\{\text{H}\}$ PENDANT NMR spectrum (101 MHz, C_6D_6 , 298 K) of $[\text{Ru}(\text{IMes})'(\text{PPh}_3)(\text{CO})\text{ZnMe}]$ (**15**).

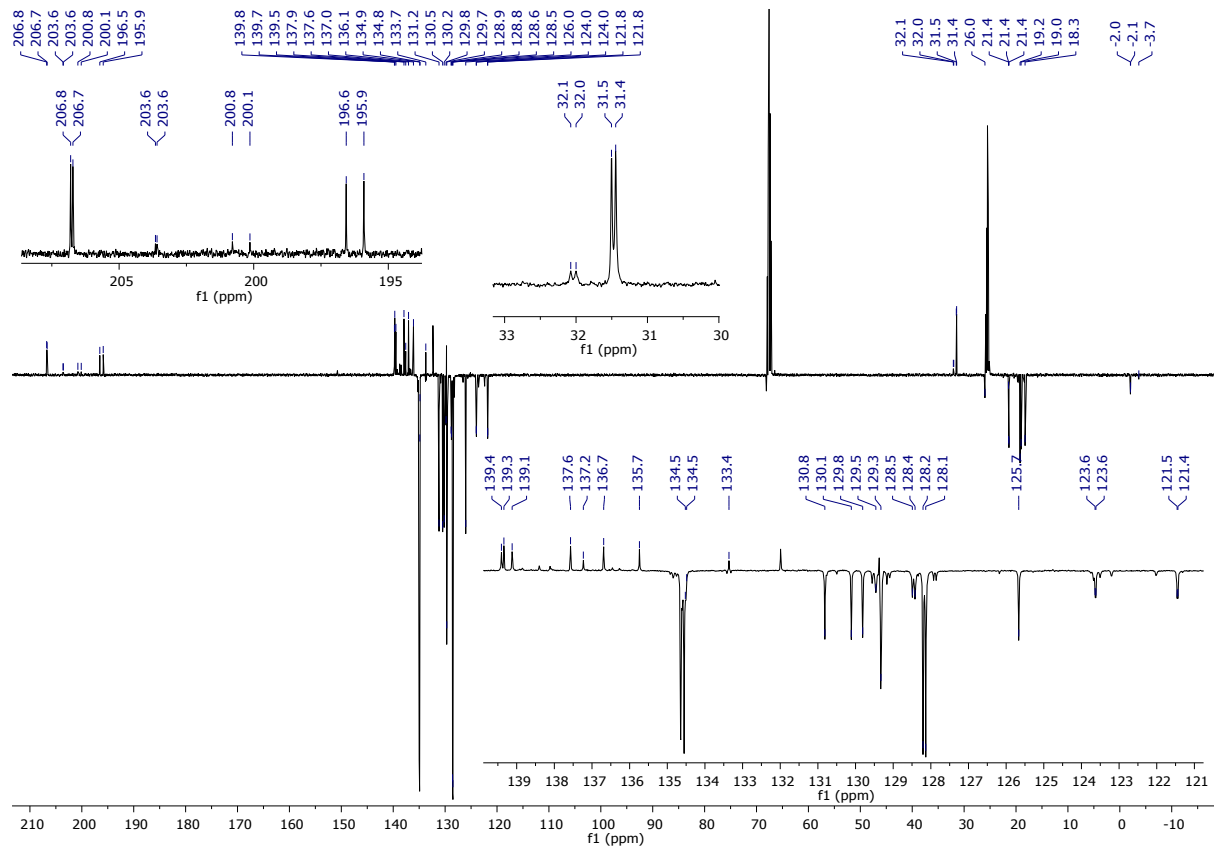
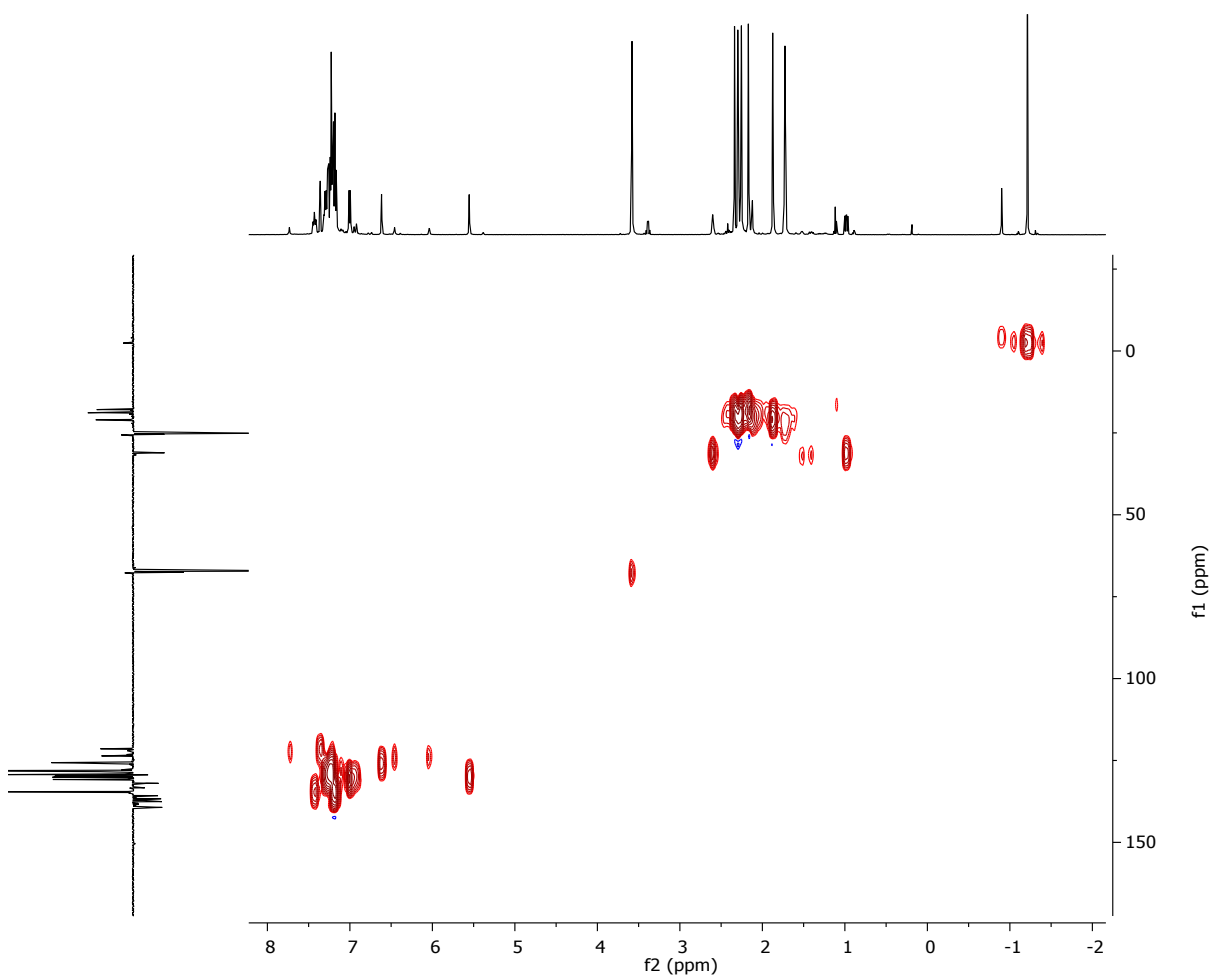


Figure S23. ^{13}C { ^1H } DEPTQ NMR spectrum (126 MHz, THF- d_8 , 298 K) of [Ru(IMes)(PPh₃)(CO)ZnMe] (**15**).



IMes cyclometallated region (Ru-CH₂):

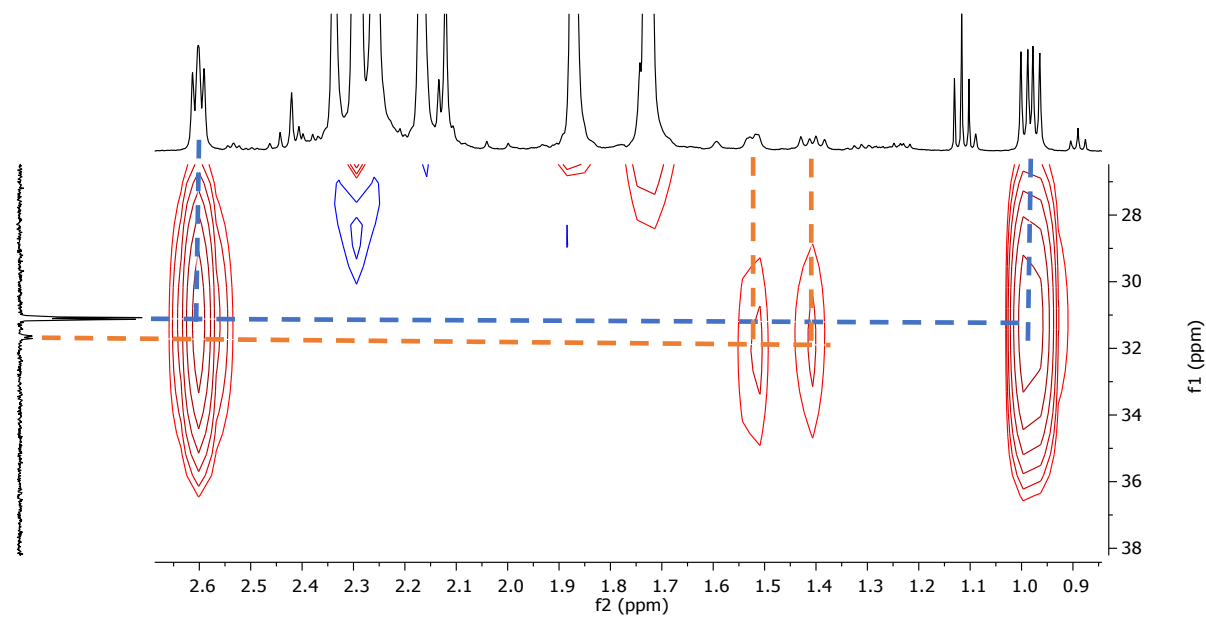
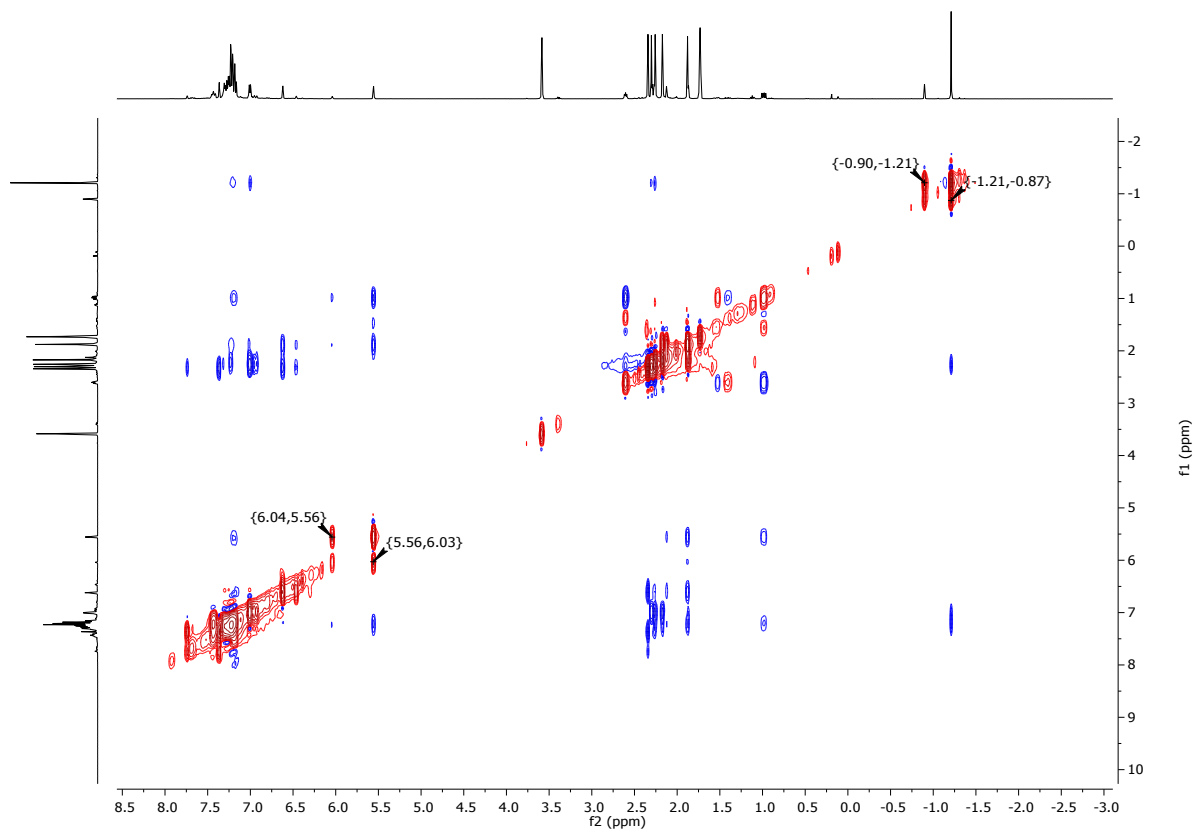


Figure S24. ^1H - ^{13}C HSQC spectra (THF- d_8 , 298 K) of $[\text{Ru}(\text{IMes})'(\text{PPh}_3)(\text{CO})\text{ZnMe}]$ (**15**).



IMes cyclometallated region (Ru-CH₂):

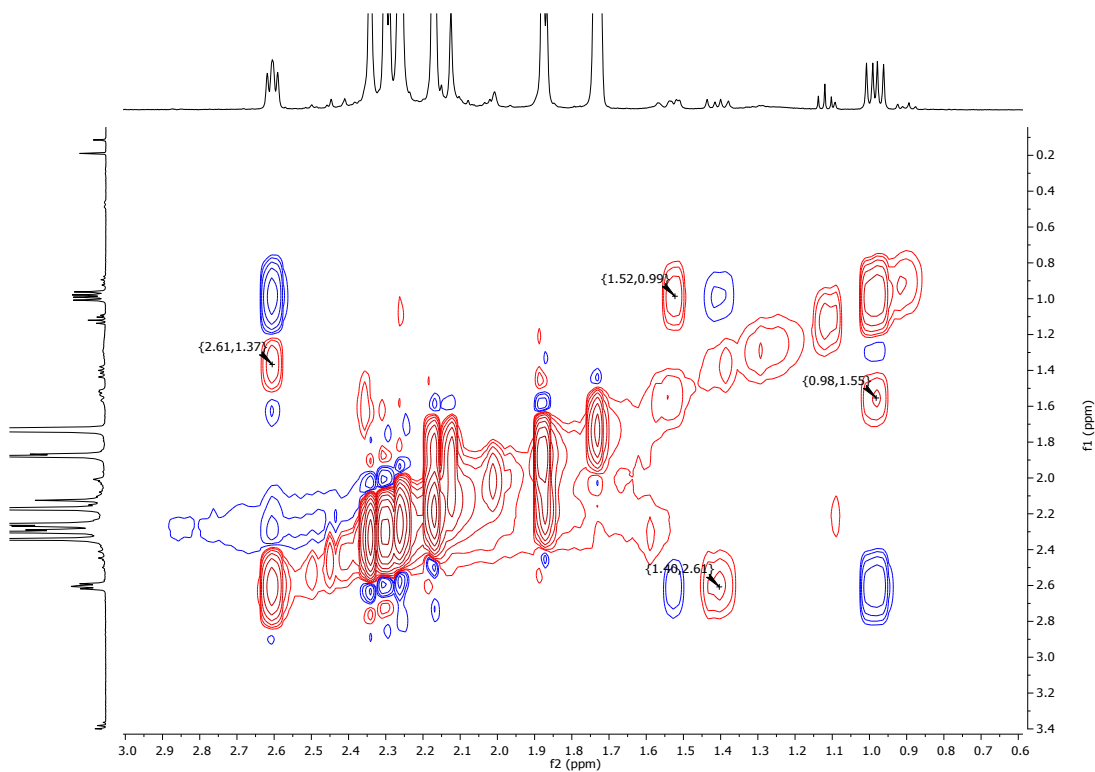


Figure S25. NOESY NMR spectra (400 MHz, THF-*d*₈, 298 K) of [Ru(IMes)(PPh₃)(CO)ZnMe] (**15**). The exchange peaks are labelled.

[Ru(IMes)(PPh₃)(CO)(ZnMe)Cl] (16). The slow, dropwise addition of ZnMe₂ (0.60 mL of 1.2 M in toluene, 0.72 mmol) to a THF (4 mL) solution of [Ru(IMes)(PPh₃)(CO)HCl] (105 mg, 0.143 mmol) brought about a colour change from yellow to dark orange. After stirring for 1 h, the volatiles were removed under vacuum and the residue treated with Et₂O (15 mL). This afforded a yellow precipitate of **16**, which was separated and dried in vacuum. Yield 20 mg (17 % yield). ¹H NMR: δ_{H} (400 MHz, C₆D₆, 298 K) 7.66-7.55 (m, 6H, PPh₃), 6.99 (br s, 9H, PPh₃), 6.79 (s, 2H, Ar), 6.76 (s, 2H, Ar), 6.18 (s, 2H, NCH=NCH), 2.43 (s, 6H, CH₃), 2.31 (br s, 6H, CH₃), 2.19 (s, 6H, CH₃), -0.51 (s, 3H, ZnCH₃). ³¹P{¹H} NMR: δ_{P} (162 MHz, C₆D₆, 298 K) 40.3 (s). Selected ¹³C{¹H} NMR: δ_{C} (101 MHz, C₆D₆, 298 K) 200.8 (d, $^2J_{\text{CP}} = 13$ Hz, Ru-CO), 192.2 (d, $^2J_{\text{CP}} = 95$ Hz, Ru-C_{NHC}), 134.7 (d, $J_{\text{CP}} = 11$ Hz, PPh₃), 129.3 (d, $J_{\text{CP}} = 2$ Hz, PPh₃), 21.3 (s, CH₃), 19.0 (br s, CH₃), -2.7 (d, $^3J_{\text{CP}} = 3$ Hz, ZnCH₃). IR (KBr, cm⁻¹): 1878 (ν_{CO}).

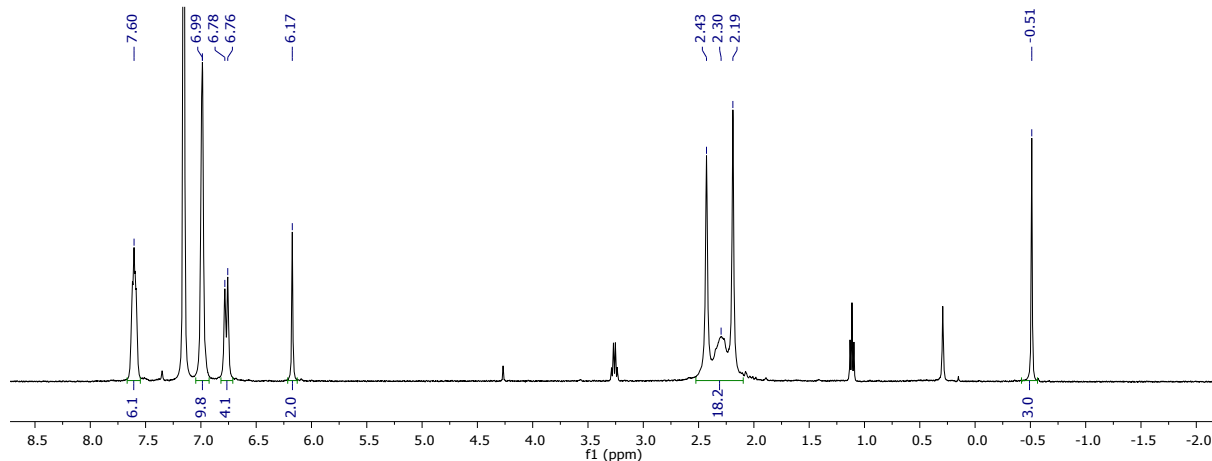


Figure S26. ¹H NMR spectrum (400 MHz, C₆D₆, 298 K) of [Ru(IMes)(PPh₃)(CO)(ZnMe)Cl] (16).

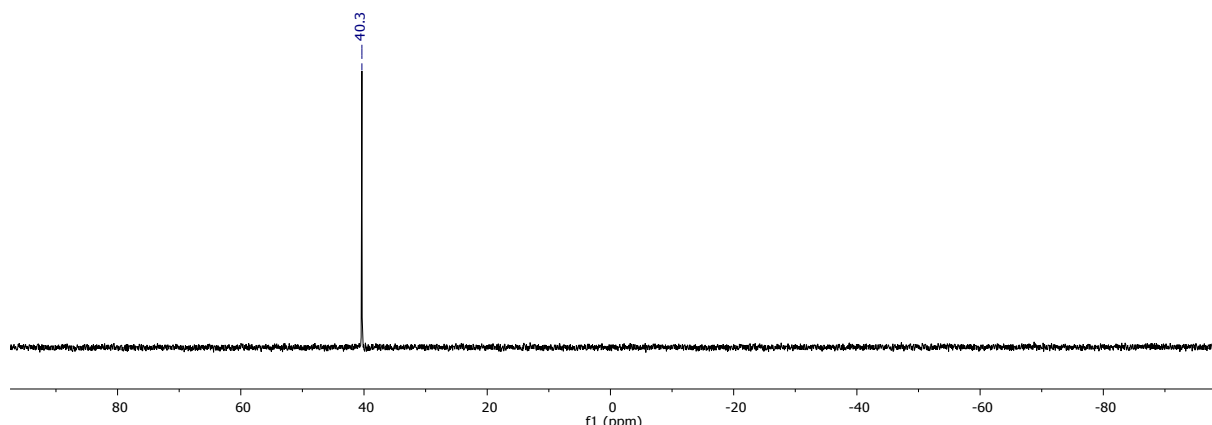


Figure S27. ³¹P{¹H} NMR spectrum (162 MHz, C₆D₆, 298 K) of [Ru(IMes)(PPh₃)(CO)(ZnMe)Cl] (16).

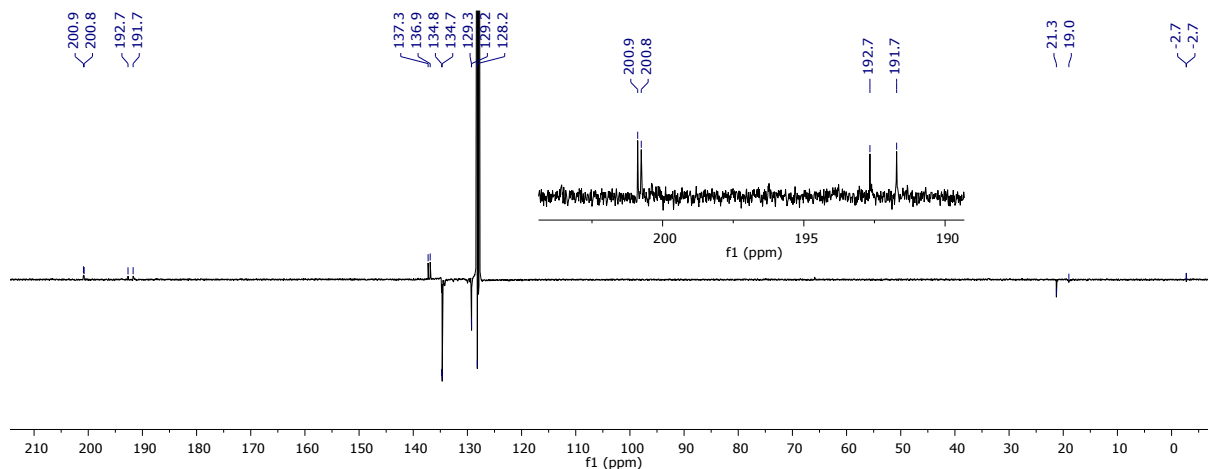


Figure S28. $^{13}\text{C}\{^1\text{H}\}$ PENDANT NMR spectrum (101 MHz, C_6D_6 , 298 K) of $[\text{Ru}(\text{IMes})(\text{PPh}_3)(\text{CO})(\text{ZnMe})\text{Cl}]$ (**16**).

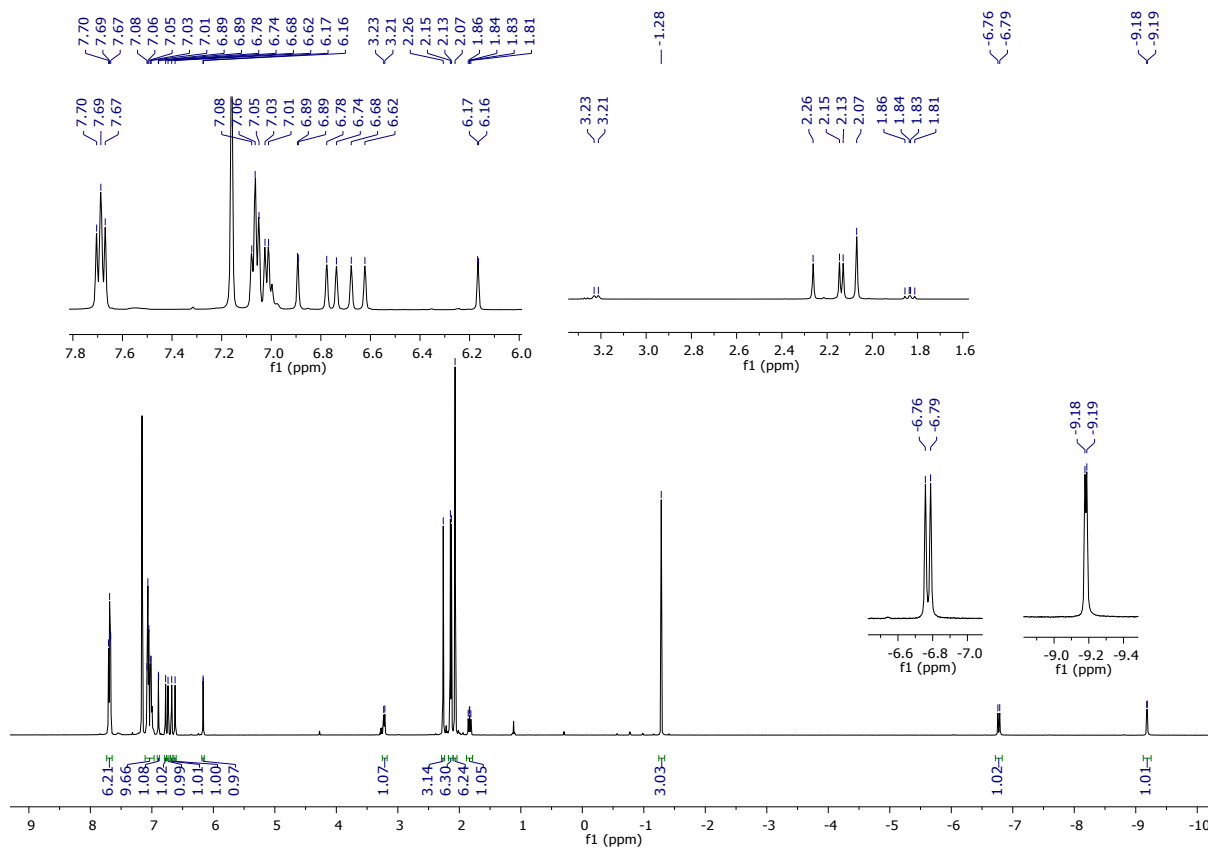


Figure S29. ^1H NMR spectrum (400 MHz, C_6D_6 , 298 K) of $[\text{Ru}(\text{IMes})'(\text{PPh}_3)(\text{CO})(\text{H})_2\text{ZnMe}]$ (17).

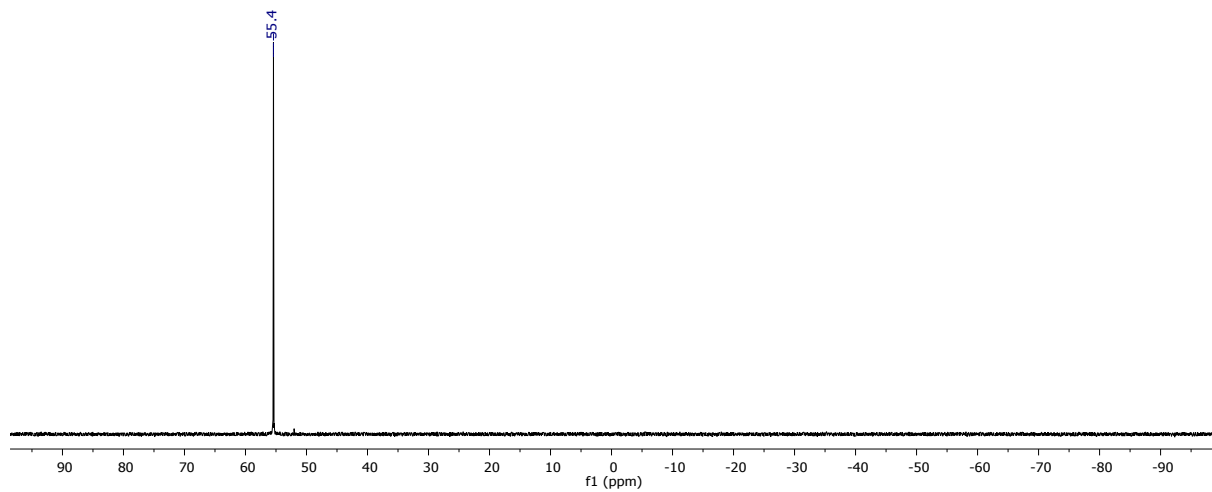


Figure S30. $^{31}\text{P}\{\text{H}\}$ NMR spectrum (202 MHz, C_6D_6 , 298 K) of $[\text{Ru}(\text{IMes})'(\text{PPh}_3)(\text{CO})(\text{H})_2\text{ZnMe}]$ (17).

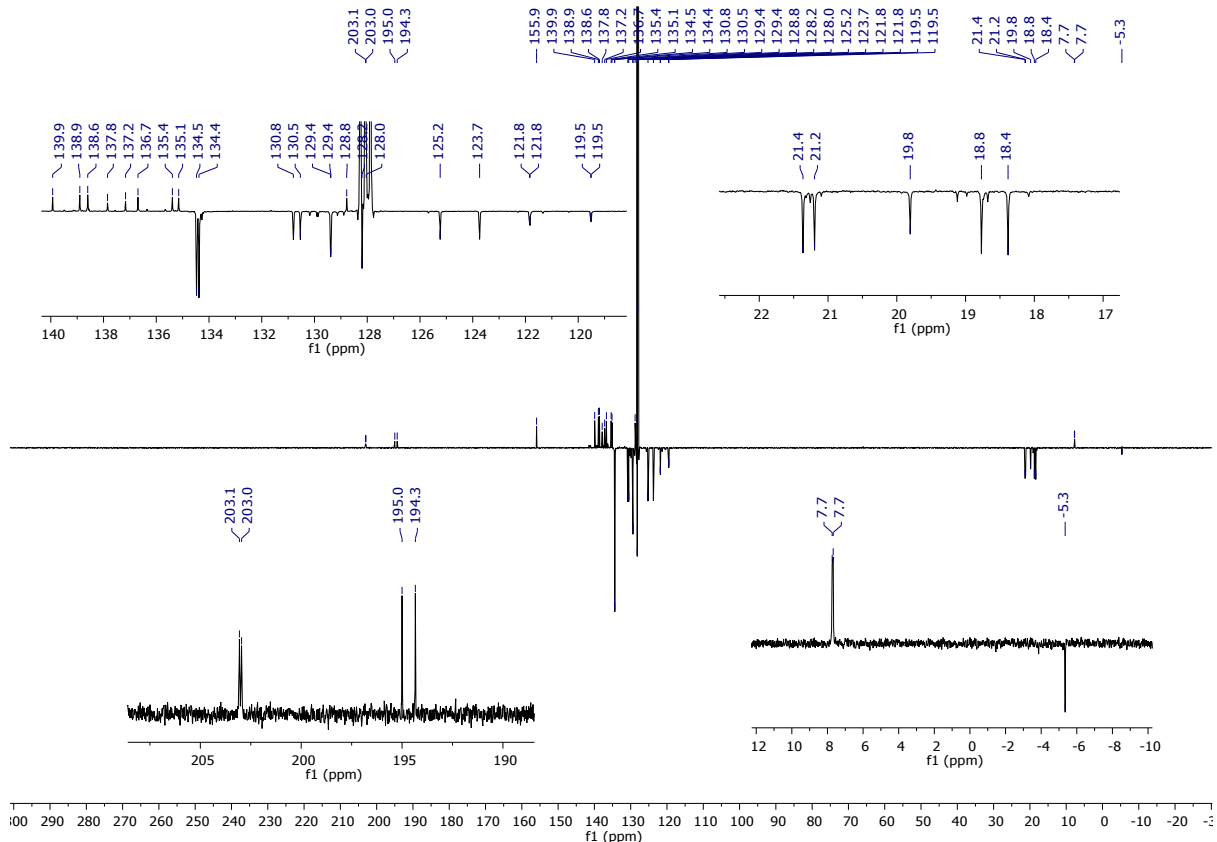


Figure S31. $^{13}\text{C}\{^1\text{H}\}$ PENDANT NMR spectrum (126 MHz, C_6D_6 , 298 K) of $[\text{Ru}(\text{IMes})'(\text{PPh}_3)(\text{CO})(\text{H})_2\text{ZnMe}]$ (**17**).

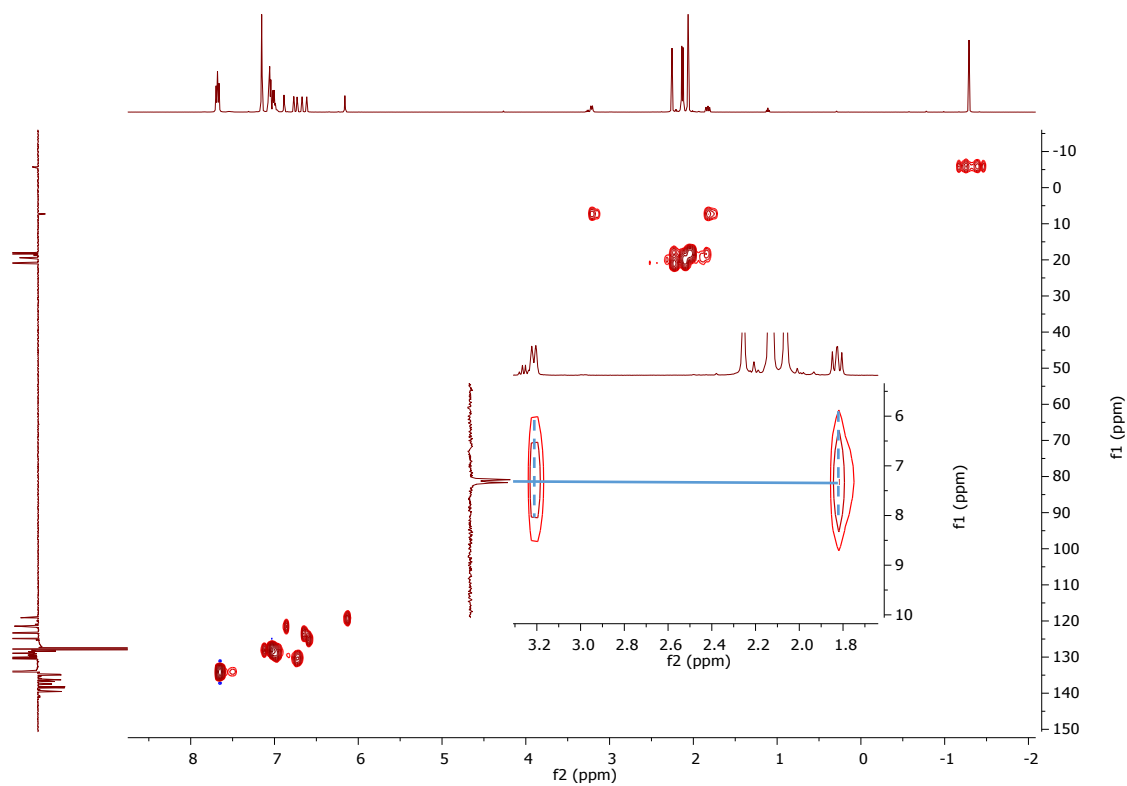


Figure S32. ^1H - ^{13}C HSQC spectrum (THF- d_8 , 298 K) of $[\text{Ru}(\text{IMes})'(\text{PPh}_3)(\text{CO})(\text{H})_2\text{ZnMe}]$ (**17**), with expansion of the cyclometallated (Ru-CH₂) region.

- U. L. Dharmasena, H. M. Foucault, E. N. dos Santos, D. E. Fogg and S. P. Nolan, *Organometallics*, 2005, **24**, 1056-1058.